Biogeosciences, 12, 5429–5454, 2015
www.biogeosciences.net/12/5429/2015/
doi:10.5194/bg-12-5429-2015

Biogeosciences Open Access

Oxygen minimum zones in the tropical Pacific across CMIP5 models: mean state differences and climate change trends

A. Cabré[1], I. Marinov[1], R. Bernardello[1,2], and D. Bianchi[3,4]

[1]Department of Earth and Environmental Science, University of Pennsylvania, Philadelphia, USA
[2]National Oceanographic Centre, Southampton, UK
[3]School of Oceanography, University of Washington, Seattle, USA
[4]Department of Atmospheric and Oceanic Sciences, University of California Los Angeles, Los Angeles, USA

Correspondence to: A. Cabré (cabre@sas.upenn.edu)

Received: 19 March 2015 – Published in Biogeosciences Discuss.: 30 April 2015
Accepted: 2 September 2015 – Published: 21 September 2015

Abstract. We analyse simulations of the Pacific Ocean oxygen minimum zones (OMZs) from 11 Earth system model contributions to the Coupled Model Intercomparison Project Phase 5, focusing on the mean state and climate change projections. The simulations tend to overestimate the volume of the OMZs, especially in the tropics and Southern Hemisphere. Compared to observations, five models introduce incorrect meridional asymmetries in the distribution of oxygen including larger southern OMZ and weaker northern OMZ, due to interhemispheric biases in intermediate water mass ventilation. Seven models show too deep an extent of the tropical hypoxia compared to observations, stemming from a deficient equatorial ventilation in the upper ocean, combined with too large a biologically driven downward flux of particulate organic carbon at depth, caused by particle export from the euphotic layer that is too high and remineralization in the upper ocean that is too weak.

At interannual timescales, the dynamics of oxygen in the eastern tropical Pacific OMZ is dominated by biological consumption and linked to natural variability in the Walker circulation. However, under the climate change scenario RCP8.5, all simulations yield small and discrepant changes in oxygen concentration at mid depths in the tropical Pacific by the end of the 21st century due to an almost perfect compensation between warming-related decrease in oxygen saturation and decrease in biological oxygen utilization. Climate change projections are at odds with recent observations that show decreasing oxygen levels at mid depths in the tropical Pacific.

Out of the OMZs, all the CMIP5 models predict a decrease of oxygen over most of the surface and deep ocean at low latitudes and over all depths at high latitudes due to an overall slow-down of ventilation and increased temperature.

1 Introduction

Most marine organisms suffer and might die in hypoxic conditions, i.e. when the oxygen concentration falls below 60–80 mmol m^{-3} (Gray et al., 2002; Stramma et al., 2008). Note that this is a limited definition, since the specific survival and performance of organisms also depend on the species, temperature, oxygen partial pressure, and CO_2 levels (Seibel, 2011). However, a definition based on oxygen concentration facilitates the comparison across models. Oxygen minimum zones (OMZs) develop on the eastern outskirts of the subtropical gyres, owing to poor ventilation combined with high biological consumption, a consequence of strong upwelling and biological productivity.

Two of the largest OMZs in the world are found to the north and the south of the equator, respectively, in the eastern tropical Pacific. The northern (Costa Rica Dome) is the largest of the two OMZs and is separated from the smaller one (west of Peru) by a well-ventilated equatorial band (Karstensen et al., 2008; Paulmier and Ruiz-Pino, 2009; Fuenzalida et al., 2009). The locations of the tropical Pacific OMZs are mostly determined by sluggish ventilation, coinciding with a maximum in water age rather than a maximum in biological productivity (Karstensen et al., 2008; Stramma

et al., 2010b). As subtropical gyres prevent a direct meridional ventilation of the OMZ, it is thought that eastward equatorial currents are the most likely sources of oxygen to the OMZs (Stramma et al., 2010b). These equatorial zonal jets are themselves fed by high-latitude water masses. The northern tropical Pacific is directly ventilated by the North Pacific Intermediate Water (NPIW), which, however, only penetrates to a depth of 600 m, resulting in severe oxygen depletion below this depth. The southern Pacific is mostly ventilated by water masses formed in the Southern Ocean, such as the Antarctic Intermediate Water (AAIW) and the Subantarctic Mode Water (SAMW), which ventilate mid-depth layers, and the Antarctic Bottom Water (AABW), which ventilates the deep ocean.

A common problem in non-eddy-resolving Earth system models is the merging of the northern and southern OMZs in the tropics, resulting in large overestimation of the OMZ volume relative to observations (Bopp et al., 2002; Matear and Hirst, 2003; Cocco et al., 2013; Stramma et al., 2010a). This is related to the "nutrient-trapping" problem in coarse-resolution models (Najjar et al., 1992), where nutrients that accumulate in the subsurface due to excessive remineralization feed the surface layers and promote new production. This maintains high remineralization rates and, in the absence of a vigorous horizontal circulation, anomalously high nutrient pools in the subsurface.

It is hard to distinguish to what extent the OMZ biases in models are driven by physical and biogeochemical processes, or a combination of both. Najjar et al. (2007) found large differences in oxygen, particulate organic carbon (POC), and dissolved organic carbon (DOC) when comparing 12 different circulation models with the same biogeochemical module. On the other hand, Kriest et al. (2010, 2012) studied the sensitivity of a fixed physical ocean model to changes in biogeochemical parameters related to oxygen loss, also finding large differences in the shape of OMZ. These studies reveal that both physical and biogeochemical causes modify the oxygen concentration and the shape of the OMZ, making it difficult to isolate the different contributions when comparing models with both different physics and biogeochemistry, as in the current study.

With climate change, increased temperatures result in decreased O_2 solubility (thermal effect) while an increase in stratification is expected to reduce the ventilation of the subsurface and hence O_2 concentration (Keeling and Garcia, 2002). Significant global deoxygenation over the past 50 years has been observed (Helm et al., 2011) together with expansion of the OMZ in the North Pacific (Ono et al., 2001; Emerson et al., 2004; Whitney et al., 2007; Chan et al., 2008; Pierce et al., 2012) and in the southern California Current System (Bograd et al., 2008; McClatchie et al., 2010), with the largest relative O_2 declines occurring below the thermocline in the tropical oceans (Stramma et al., 2008, 2010b, 2012). While observations show a clear ongoing decline of oxygen in the tropical thermocline, previous Earth system model studies show a small change or even an increase of oxygen there with warming (Bopp et al., 2002, 2013; Matear and Hirst, 2003; Cocco et al., 2013), with a small associated change in OMZ volume. The expansion of low-oxygen zones will result in the transition, adaptation, and/or extinction of different species in the real ocean.

The wide range of physical and biogeochemical characteristics across CMIP5 models offers a unique opportunity to understand common and persistent biases in state-of-the-art resolution Earth system simulations. In this study, we analyse 11 Earth system models participating in the Coupled Model Intercomparison Project Phase 5 (CMIP5, Taylor et al., 2012) to identify the common mechanisms involved in the creation of OMZ biases in the eastern tropical Pacific, as well as the response of the respective OMZs to interannual variability and climate change. We compare models with observations, analyse potential sources of bias across different models, and provide recommendations for improving OMZ representation. Methods are described in Sect. 2. Results are summarized in Sect. 3 and include historical biases in the description of Pacific OMZs across CMIP5 models (Sect. 3.1), 21st century predictions (Sect. 3.2), and interannual variability (Sect. 3.3). The full, model-by-model analysis of the physical and biological processes influencing the position and extension of OMZs is presented in the Appendix. Based on literature review and our own analysis, we summarize in Tables A2 and A3 descriptions of (a) relevant ventilation sources and (b) biochemical parameters and processes that affect OMZs across the CMIP5 models analysed.

2 Methods

2.1 Earth system simulations

We examine simulations from 11 non-eddy-resolving CMIP5 Earth system models, downloaded from http://pcmdi9.llnl.gov/esgf-web-fe/(detailed in Table A1). In order to estimate 100-year trends, our analysis compares simulations for the period 1960–1999 (hereafter called "present") to simulations for the period 2060–2099 (hereafter called "future"). We assume that the 40-year periods are sufficiently long to ensure that natural variability is smoothed out. The historical period is chosen around 1980 for a direct comparison to observations. The "present" output is taken from the "historical" experiment (years 1850 to 2005), while the "future" output is taken from the Representative Concentration Pathway 8.5 experiment (hereafter called RCP8.5, years 2006 to 2100), detailed in Meinshausen et al. (2011). Atmospheric CO_2 concentrations are based on observed and reconstructed values for the historical experiment, while RCP8.5 values are based on CO_2 emissions resulting in a radiative forcing of $8.5\,W\,m^{-2}$ by the end of the 21st century (Riahi et al., 2011).

Our selection of models was then limited to those that included the variable "O_2" (oxygen concentration) and out-

put for both the historical and RCP8.5 experiments, and had reached equilibrium (no significant trends during the period 1850–1950). One of the analysed models, MRI-ESM1, did not provide RCP8.5, so the ESM RCP8.5 scenario, which explicitly computes CO_2 levels from anthropogenic emissions (Friedlingstein et al., 2014), was used instead in this case. For Sect. 3.3, we created a control time series to study natural interannual variability by de-trending the historical run from 1900 to 1999 from its climate signal (calculated as the 20-year running mean).

2.2 Observations

We used oxygen (O_2), apparent oxygen utilization (AOU), saturated oxygen (O_2sat), nitrate, phosphate, salinity, and temperature climatologies from the World Ocean Atlas 2009 database (https://www.nodc.noaa.gov/OC5/WOA09/pr_woa09.html). We applied a correction to oxygen concentrations which were found to be overestimated in gridded World Ocean Atlas (WOA) data (Bianchi et al., 2012). Sea level pressure was provided by the NOAA/OAR/ESRL PSD data set at http://www.esrl.noaa.gov/psd/ (Kaplan et al., 2000). Water-mass age (year) was calculated from radiocarbon deficit (^{14}C (‰)), downloaded from the Global Ocean Data Analysis Project database (http://cdiac.ornl.gov/oceans/glodap/), as age $= -8033 \ln(1 + {}^{14}\mathrm{C}/1000)$. Since we only use it as a qualitative reference, there is no need for further calibration. The climatology of the equatorial component of the water current velocity (u (m s^{-1})) was taken from Johnson et al. (2002).

In order to compare models with observations, we calculated for each model simulation O_2sat from the in situ temperature and salinity (Garcia and Gordon, 1992); O_2sat represents the oxygen concentration in equilibrium with the atmosphere at a given temperature and salinity. The apparent oxygen utilization (AOU) was then computed as the difference between O_2sat and O_2 (AOU = O_2sat-O_2). AOU for a parcel of water represents the accumulated oxygen consumption since the parcel left the surface along the ventilation pathway, assuming that O_2 was saturated at the time the parcel was last in contact with the atmosphere. We note that AOU is not the real oxygen consumption, given that most waters are undersaturated in zones of deep-water formation (Ito et al., 2004), but it provides a good approximation.

Particulate organic carbon export was obtained from satellite-derived estimates calibrated with in situ export measurements from shallow traps (Dunne et al., 2005) and thorium-based methods (Henson et al., 2012), and by combining satellite observations and food-web models in Siegel et al. (2014).

For both models and observations, stratification was calculated as the difference in the potential density (kg m^{-3}) of seawater between the depth of 200 m and the surface. The Walker circulation index was defined as the difference between the sea level pressure at the eastern tropical Pacific (160–80° W and 5° S–5° N) and the western tropical Pacific (100–160° E and 5° S–5° N) as in Vecchi et al. (2006).

2.3 Agreement across models

The multi-model mean is calculated as the average value across all the CMIP5 models in the period 1960–1999, with a simple weight applied to avoid repeating models that are known to be very similar (Table A1, Cabré et al., 2015).

To quantify agreement among the models in the predicted 100-year change, we use a bootstrapping statistical technique. In our bootstrap sampling, each realization is the weighted average over N models that are selected randomly with replacement among the N available models. We represent interannual variability by randomly picking one of the 40 years in the present (1960–1999) and future (2060–2099) each time that we randomly select a model. For each studied variable at each point in the ocean, we create 1000 realizations of the resulting 100-year trend and obtain the multi-model significance of this trend using the percentage of realizations that predict a trend above or below zero (details in Cabré et al., 2015).

3 Results and discussion

3.1 Comparison of observed and predicted OMZs in the CMIP5 models during the historical period (1960–1999)

The comparison between CMIP5 model oxygen simulations and WOA09 observations highlights several consistent biases (Fig. 1 and 2a). (a) The majority of the models join the northern and southern OMZ regions into a single large tropical OMZ (Fig. 1a), such that the modelled OMZ reaches anoxic conditions at shallower depths (Fig. 1c–d), and expands more westward and deeper than observed (Fig. 1c–d). (b) In observations, the northern OMZ area and volume are much larger than the southern counterpart, while in models, the northern and southern OMZ areas and volumes are much more symmetric with respect to the equator (Fig. 1a–b). A reason for this is a bias in the modelled Southern Hemisphere OMZ, systematically larger than observed except for the IPSL models (Fig. 1a–c, Fig. 2). In addition, in some models (namely, GFDL-ESM2G, GFDL-ESM2M, HadGEM2, NorESM1-ME, and MRI-ESM1) the Northern Hemisphere OMZ is often too small in horizontal extent or does not extend as deep as in observations (Fig. 2). (c) A subset of models (GFDL-ESM2G, GFDL-ESM2M, MPI-ESM, and NorESM1-ME) produce anoxia to a depth of 2500 m or more in the eastern tropical Pacific, which is deeper than observations by more than 1500 m (Fig. 1c–d and 2).

Figure 3 shows the modelled and observed vertical distributions of oxygen, phosphate, and nitrate averaged over the eastern tropical Pacific (a, b, c) and the world ocean (d, e, f). Note the large dispersion of the modelled values in

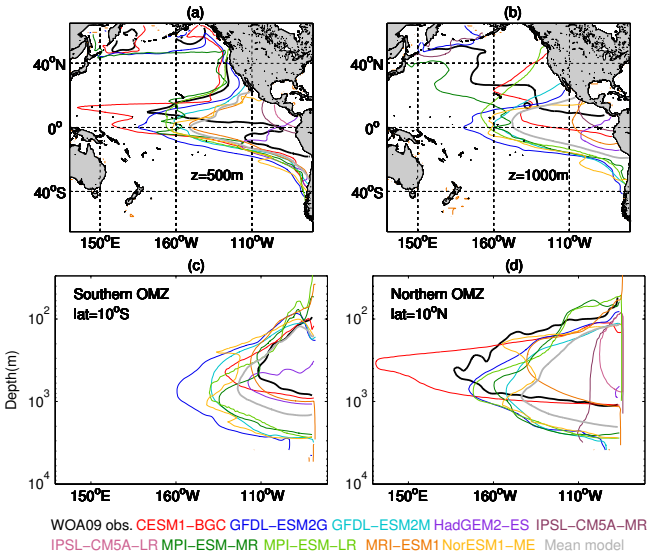

Figure 1. Comparison of the Pacific Ocean oxygen minimum zones (at $O_2 = 30\,\mathrm{mmol\,m^{-3}}$) across CMIP5 models (represented by coloured lines – see legend for explanation) and observations (solid black lines) during the historical period 1960–1999. The grey line represents the multi-model mean, calculated using the weights in Table A1. Panels **(a)** and **(b)** show the OMZs at depth 500 and 1000 m, while panels **(c)** and **(d)** show longitudinal depth sections of the Southern and Northern tropical OMZs, at latitude 10° S and 10° N. Depth scale (m) is logarithmic. The model HadGEM2-CC (not shown) shows results similar to HadGEM2-ES.

the eastern tropical Pacific despite a good agreement on the global scale. Models that simulate anomalously deep OMZs yield oxygen levels at intermediate depths that are too low compared to observations and too much phosphate trapped at great depths. Concurrently, such low levels of oxygen in these models trigger denitrification, reducing nitrate to anomalously low levels.

We discuss in the following the main potential causes for the aforementioned biases. The full, model-by-model analysis of the physical and biological processes influencing the position and extension of OMZs is presented in detail in Appendix 1 and Tables A1, A2, and A3.

3.1.1 Physical causes for OMZ biases in historical simulations

In this section we explore differences between models and observations in ventilation patterns, mixing coefficients, and ocean-model resolution – all of these possible physical causes for OMZ model biases.

Underestimated Equatorial Undercurrent

The complex system of equatorial currents is dominated by the Equatorial Undercurrent (EUC), the strong subsurface eastward current shown in observations in the last panel of Fig. 4. On the one hand, the EUC determines the depth of the tropical Pacific OMZ in the west–east direction and controls most of the ventilation with O_2 to the tropical OMZ (Aumont et al., 1999). On the other hand, the EUC is responsible for bringing the nutrients that enhance biological productivity and subsequent consumption of organic matter on the eastern side of the basin, contributing to OMZ formation and opposing the ventilation effect. As an example, the underestimate of subsurface OMZ volume in the IPSL-CM5A models (Fig. 1a–b) might be related to the fact that nutrients (and hence primary production and POC flux) are underestimated there when compared to the rest of CMIP5 models (Fig. 3b and 5), probably due to a weak EUC (Fig. 4).

All CMIP5 models show that EUC weakens too much before reaching the eastern side of the basin (Fig. 4), which contributes to weaker eastern ventilation compared to observations. However, we find that the models which have the most accurate representations of the EUC flow (NorESM1-ME and MPI-ESM-MR) still produce OMZs that are too large, pointing to other causes for OMZ bias. Despite the bias in EUC strength, the EUC is better modelled than the rest of the equatorial currents and it is not thought to be the main cause for the large OMZ across simulations (Dietze and Loeptien, 2013). A comparison between EUC flow and Pacific OMZ size at mid-depths across CMIP5 models showed no correlation.

Increased resolution improves the representation of equatorial currents (especially the EUC; Aumont et al., 1999), which is evident when comparing MPI-ESM-LR (coarse-resolution model) and MPI-ESM-MR (quasi-eddy-resolving resolution, 0.4°) in Fig. 4 (see also Jungclaus et al., 2013). However, both versions of the MPI-ESM model show similar biases in oxygen distribution and a tropical OMZ that is too deep (Fig. 1), which suggests that the OMZ that is modelled as being too deep is not linked to the strength of equatorial currents, but set by high-latitude ventilation processes or/and biological biases at low latitudes. Both IPSL-CM5A models, with low ocean resolution of $\sim 2°$, show similarities to MPI-ESM-LR (same $\sim 2°$ resolution) in the characterization of a diffuse and weak EUC and non-existent deep jets. The rest of the models have an oceanic resolution of $\sim 1°$, higher than that of IPSL-CM5A and MPI-ESM-LR models (Table A1), and hence provide a more accurate representation of EUC compared to observations.

Deficient equatorial (non-EUC) ventilation

In general, the non-EUC equatorial jets are also too weak or in some cases non-existent in non-eddy-resolving models (compare CMIP5 models and observations in Fig. 4). This complex equatorial system is formed by the eastward Northern and Southern Equatorial countercurrents (NECCs and SECCs) and Northern and Southern Subsurface countercurrents (NSCCs and SSCCs, also known as Tsuchiya jets in the Pacific; Tsuchiya, 1981) – shown as currents at 6–8° N

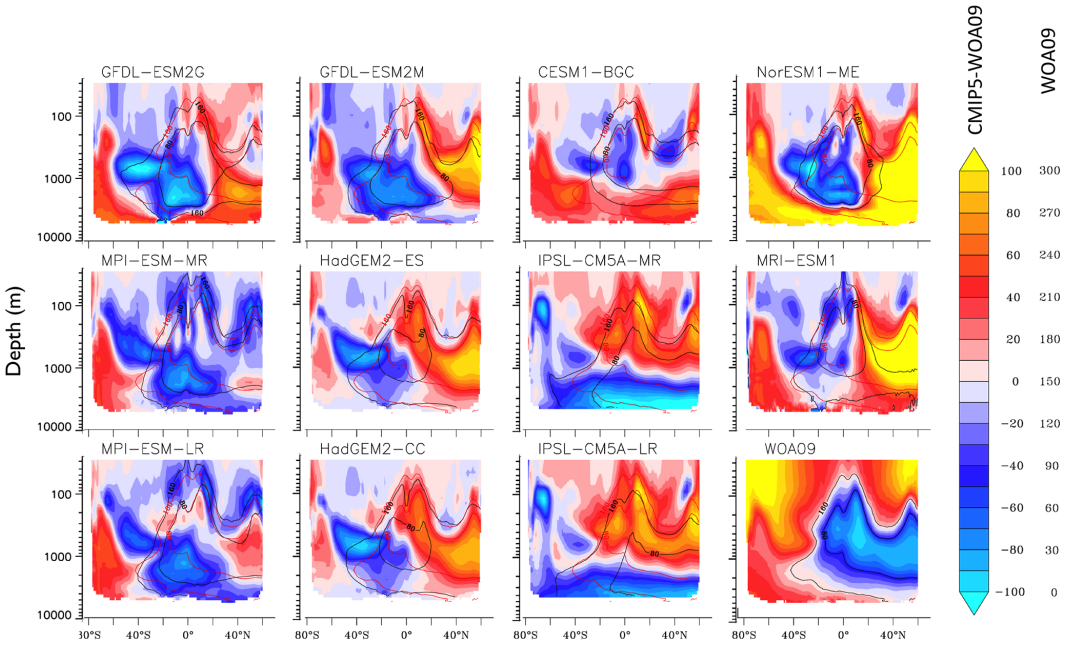

Figure 2. Differences between CMIP5 models' estimates and WOA09 climatological observations of oxygen concentration (mmol m^{-3}) zonally averaged from 160 to 60° W in the Pacific at various depths and latitudes during the historical period (1960–1999). The last panel shows the corresponding zonal mean oxygen concentrations (mmol m^{-3}) from the observational WOA09 data set. In each panel, oxygen concentrations equal to 80 and 160 mmol m^{-3}, respectively, are represented by superimposed contour lines (black for each model and red for observations).

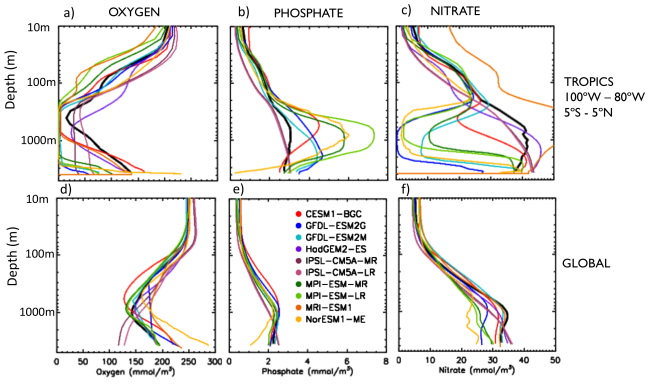

Figure 3. Average vertical profiles of **(a)** oxygen, **(b)** phosphate and **(c)** nitrate concentrations (mmol m^{-3}) from CMIP5 models (coloured lines – explained in the legend) and the WOA09 observations (black line) in the eastern tropical Pacific region, spanning 80 to 100° W longitude and 5° N to 5° S latitude. **(d)**–**(f)** Analogous global averages. The model HadGEM2-CC (not shown) shows results similar to HadGEM2-ES.

and 6–8° S in the last panel of Fig. 4, the westward northern and main branches of the South Equatorial Current (SEC(N) and SEC) – on both sides of the EUC in Fig. 4, and deeper currents as described in detail, for example in Stramma et al. (2010b).

In observations, the Northern and Southern Equatorial and Subsurface Countercurrents (ECCs and SCCs) determine the separation between the well-ventilated tropics and the low-latitude OMZs (Fig. 1a). However, because of the deficient equatorial circulation in the models (Fig. 4), most models tend to join the northern and southern OMZ cells – well separated in observations – into a single large tropical OMZ (Fig. 1a). We suggest that consequences of the lateral ventilation of these regions being too slow in CMIP5 models include subsurface oxygen concentration being too low(Fig. 3a) and nitrate depletion that is too large due to excessive denitrification kicking in when O_2 falls below a certain threshold (Fig. 3c, compare black and coloured lines). The low ventilation exacerbates nutrient trapping and potential for runaway feedbacks in the nitrogen cycle (Landolfi et al., 2013). The CMIP5 models also underestimate the strength of westward subsurface equatorial jets (SECs), which in the real ocean contribute to carrying nutrients away from the OMZ, thus alleviating the large oxygen deficit and nutrient trapping in the tropical OMZ. Finally, CMIP5 models do not capture the fine structure of the deep equatorial jets, thus underestimating lateral advection and mixing along the equator and contributing to the expansion of OMZs. Consequently, all models except for the IPSL-CM5A models show a subsurface excess of phosphate in the Pacific tropics (Fig. 3b). Dietze and Lopetien (2013) also speculate that nutrient trapping is caused by a poor representation of the

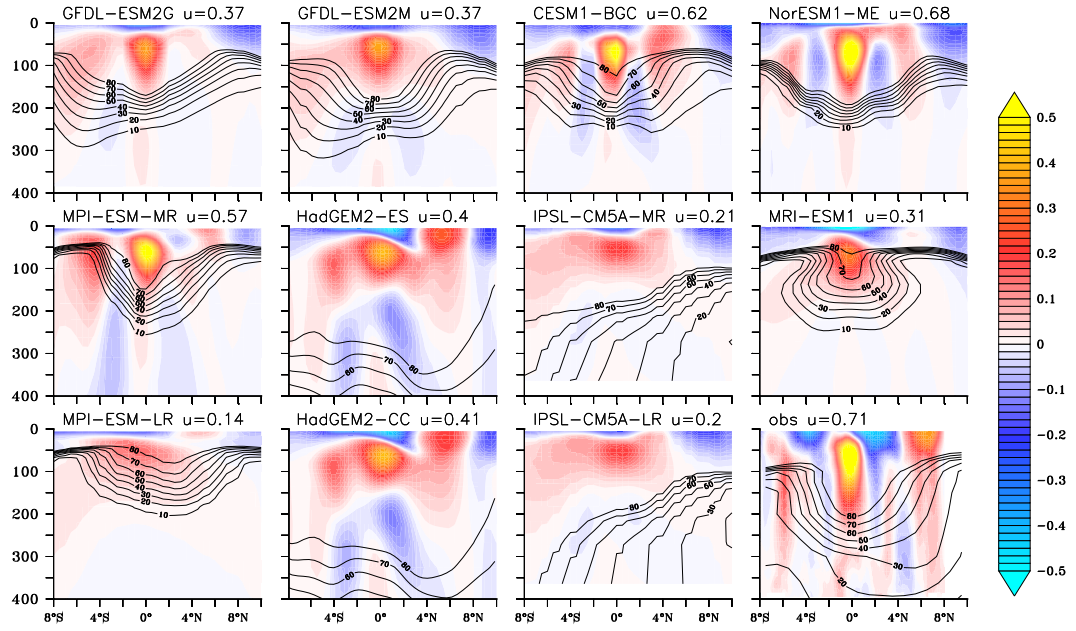

Figure 4. Average equatorial ventilation (represented by the zonal component of velocity, m s^{-1}, shown in colours) and oxygen concentration (shown as black contour lines for 10, 30, 40, 50, 60, 70, and 80 mmol m^{-3}, respectively) in CMIP5 models and observations (last panel), with depth along a 95° W longitude section in the tropical west Pacific (10° N to 8° S latitude). Observed u velocity is from Johnson et al. (2002) while the oxygen observations are from WOA09. The dominant current shaping the OMZ in the east–west direction is the Equatorial Undercurrent, revealed by the high (red to yellow) velocities at the equator. The maximum intensity of the EUC is labelled next to the model name (in m s^{-1}).

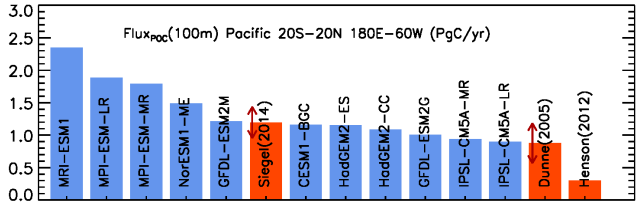

Figure 5. Total particulate organic carbon (POC) flux (Pg/year) at the depth of 100 m in the eastern tropical Pacific (20° S to 20° N latitude and 180° E to 60° W longitude) estimated by each of the CMIP5 models (blue) and derived from measurements (orange) by Dunne et al. (2005), Henson et al. (2012), and Siegel et al. (2014). Results are ordered according to the flux magnitude. Dunne et al. (2005) reported errors of 35 % and Siegel et al. (2014) errors of 20 % (shown as arrows).

equatorial current system in models, with the exception of the EUC. Montes et al. (2014) show the crucial role of the secondary Tsuchiya jet (sSSCC, subsurface current at ∼ 9° S) in the ventilation of the OMZ off Peru. A good balance between oxygen-poor transport by sSSCC and oxygen-rich transport by EUC is crucial to describe the position and extent of this OMZ. Similarly, Duteil et al. (2014a) highlight the need for accurate deep equatorial ventilation, in addition to EUC, to characterize the eastern tropical Atlantic OMZ.

Some recent studies showed that the equatorial ventilation is not fully resolved even in eddy-resolving models (Brandt et al., 2008; Eden and Dengler, 2008; Ascani et al., 2010), suggesting that other mechanisms such as submesoscale dynamics, or atmosphere–ocean feedbacks might also be responsible for biases in the equatorial jets and their incomplete representation in models (Lin, 2007; Li and Xie, 2014; Ridder and England, 2014).

Inadequate ventilation from the Southern Ocean and North Pacific

The Pacific Ocean equatorial circulation is fed by intermediate water masses formed in the Southern Ocean (AAIW, SAMW) and North Pacific (NPIW). In observations, the northern tropical Pacific OMZ is larger and deeper than the OMZ south of the equator, because the former receives disproportionately less oxygen via the large-scale circulation pathways (Karstensen et al., 2008).

Sallee et al. (2013b) reported large variations in the formation of Southern Ocean water masses across CMIP5 models. We find also considerable inter-model variability in the zonally averaged vertical distribution of oxygen (Fig. 2). Most CMIP5 models overestimate the size of the southern tropical Pacific OMZ, which develops at shallower depths than observed (Fig. 1c), partly due to deficient intermediate water ventilation from the Southern Ocean, reinforced by exces-

sive biological export and remineralization. Previous studies have pointed out that, in current coarse-resolution models, the AAIW and SAMW do not extend sufficiently northward in the Pacific (Sallee et al., 2013b; Downes et al., 2010), in agreement with our findings.

Some models (namely, GFDL-ESM2G, GFDL-ESM2M, HadGEM2, NorESM1-ME, and MRI-ESM1) overestimate oxygen levels north of the tropical OMZ in addition to underestimating oxygen in the low latitudes of the Southern Hemisphere (Fig. 2). The observed deep anoxic zones in the Northern Hemisphere (at depths between 600 and 1200 m) are not found in these models due to excessively deep ventilation by AABW-fed flow from the Southern Ocean to the deep North Pacific and/or an excessive mixing of NPIW with deep waters (see details and references for individual models in Table A2). For example, models with excessively deep AABW ventilation (such as NorESM1-ME and GFDL-ESM2G) or excessive NPIW ventilation (such as GFDL-ESM2M) have a reduced extent of the North Pacific OMZ. On the other hand, deficient NPIW ventilation, as in CESM1-BGC, exaggerates the volume of OMZs in the Northern Hemisphere (Fig. 2 and Table A2).

However, the anomalously deep OMZ found in some models in the tropics (Fig. 1c–d and 2) does not seem related to ventilation sources such as AABW, AAIW, or NPIW, as models having a similar biogeochemical module (MPI-ESM and NorESM1-ME) show similar OMZ extent despite having significantly different representations of different water masses (Appendix Table A2). For example, NorESM1-ME shows one of the highest deep O_2 levels but still develops a deep OMZ (Fig. 2). This problem is discussed in Sect. 3.1.2.

Inadequate representation of isopycnal mixing

Gnanadesikan et al. (2013) proposed that models using a higher-than-observed lateral eddy diffusion coefficient (A_{redi}) simulate a higher diffusive flux of O_2 from the west along the equatorial Pacific, thereby reducing the modelled OMZ volume. However, our comparison showed no correlation between the reported A_{redi} coefficients (Table A2) and Pacific OMZ volumes across CMIP5 models. This suggests that either model differences are not primarily due to lateral mixing or, more likely, that it is not possible from this set of models alone to distinguish the effect of mixing from other parameters in the system. In particular, of the two models with the largest A_{redi} ($1000\,\mathrm{m\,s^{-12}}$), IPSL-CM5A agrees with the expectation showing low subsurface anoxia, but MPI-ESM models disagrees with the expectation by displaying a large OMZ.

Inadequate representation of diapycnal mixing

Duteil and Oschlies (2011) found that OMZs were progressively smaller at low and large background vertical diapycnal diffusivity coefficient K_{v} (above and below $K_{\mathrm{v}} = 0.2\,\mathrm{cm^2\,s^{-1}}$). At high diffusivities, the OMZs are well ventilated. At low diffusivities, the OMZs are not well ventilated but the consumption of oxygen is low because there is not much biological activity. Only at intermediate coefficients, the OMZs are large due to high consumption combined with relatively low ventilation. Among CMIP5 models, MPI-ESM, IPSL-CM5A, and GFDL-ESM2M assume a background value of $K_{\mathrm{v}} = 0.1\,\mathrm{cm^2\,s^{-1}}$ in the tropics, while models CESM1-BGC, NorESM1-ME, HadGEM2, and GFDL-ESM2G assume a value of $K_{\mathrm{v}} = 0.01\,\mathrm{cm^2\,s^{-1}}$. According to the findings by Duteil and Oschlies (2011), the former three models should have a larger OMZ compared to the last four models. However, we do not see this expected tendency across CMIP5 models.

3.1.2 Biological causes for OMZ biases in historical simulations

The main biological drivers of biases in the simulation of OMZs are biases in the export of particulate organic carbon (POC) at 100 m depth, the transfer efficiency of POC from 100 m to depth (defined as the POC export at a given depth divided by POC export at 100 m), and the way POC is treated at the sea floor (Kriest et al., 2010, 2012). We also considered the effect of the variability in models' O_2 : nutrient ratios since these ranges from 150 to 172 (in the case of the O_2 : P ratio). However, we could not find any direct correlation with OMZ biases.

Finally, we considered the effect of DOC variability across models. The range of observed DOC in the low-latitude Pacific is 65–80 $\mathrm{mmol\,m^{-3}}$ in the upper 200m, decreasing with depth to background concentrations of less than 40 $\mathrm{mmol\,m^{-3}}$ below 1000 m (Hansell, 2013). The CMIP5 models that reported DOC (all models but HadGEM2) show very diverse ranges of concentrations but in general they underestimate the observed values by 20 to 55 $\mathrm{mmol\,m^{-3}}$ in the upper 200 m. Exceptions are the GFDL-ESM2 models that have realistic vertical distributions of DOC at low latitudes. In order to achieve the right distribution of DOC, models should have at least two DOC compartments (as only GFDL-ESM2 models do), one labile and one refractory. Most of the DOC in the ocean is in a refractory or unavailable form with estimated turnover timescales of centuries to millennia (Hansell, 2013), while the remaining DOC is in a labile and reactive form with short turnover timescales. Higher concentrations of dissolved organic matter, in general, allow for nutrient export out of the production region, decreasing the local consumption of oxygen. However, we do not see any correlation between levels of DOC and hypoxia in CMIP5 models. For example, the GFDL models, with a good representation of DOC, show more hypoxia than most models that underestimate DOC.

Biased export of POC at 100 m depth

A deep OMZ could be caused by an anomalously high POC flux at 100 m depth, which in turn can be due to excessive primary productivity, excessive nitrogen fixation by diazotrophs, or excessive relative abundance of large phytoplankton, which are major contributors to sinking POC. For the CESM1 model, Moore and Doney (2007) found that simulated POC export in the Pacific is primarily driven by upwelling (nutrient supply) and less by nitrogen fixation, suggesting that the model representation of diazotrophs probably does not affect the level of anoxia in this model and probably in the rest of models with similar biogeochemistry (Table A3).

In order to quantify model biases, we considered three different POC export observational estimates for our area of study (20° S to 20° N and 180° E to 60° W in the Pacific Ocean). We compare these database estimates with our modelled POC in Fig. 5 (See Fig. S1 in the Supplement for a map of export fluxes). When compared to satellite-derived estimates based on sediment traps and thorium (Dunne et al., 2005) or estimates from satellite observations combined with food-web models (Siegel et al., 2014), at least four models predict values of POC flux that are too high (assuming errors of 35 % in Dunne et al. (2005) and 20 % in Siegel et al. (2014) as reported). However, all CMIP5 models predict POC values significantly above thorium-derived satellite estimates by Henson et al. (2012). An overestimate of export at 100 m depth contributes to anomalously deep OMZ in the MPI-ESM and NorESM1-ME models. GFDL-ESM2M and GFDL-ESM2G, with POC flux at 100 m depth consistent with observations, still develop a deep OMZ, probably due to a biased transfer of POC to depth, as discussed next. MRI-ESM1 overestimates the sinking POC flux from the surface and hence overestimates remineralized nitrate throughout the water column (Fig. 3c), but attains realistic oxygen levels by remineralizing a high proportion of the organic matter near the surface. The remaining models predict POC flux values in accordance to Dunne et al. (2005) and Siegel et al. (2014).

Biased transfer efficiency of POC from 100m to depth

A transfer of POC flux from upper layers to deeper layers that is too large would cause remineralization to occur too deeply, hence leading to phosphate trapping and too much oxygen and nitrate consumption in the deep ocean. Therefore, most remineralization should ideally take place right below the euphotic zone in order to avoid the formation of OMZs that are too deep.

Thorium-derived POC export and POC flux to deep-sea sediment traps (Henson et al., 2012) indicate that the transfer efficiency of POC from the euphotic (100 m) to deeper layers is higher at low latitudes than high latitudes (Fig. S2). However, newer measurements using neutrally buoyant sediment traps at intermediate depths suggest a correlation between high temperature and high remineralization, resulting in low transfer efficiency of POC to intermediate depth at low latitudes or high temperatures (Marsay et al., 2014). The discrepancies in these two observational results are due to data sparseness and measurements coming from different depths. This suggests that the POC profiles should not only be fitted with power laws or exponentials as traditionally done, but with a more sophisticated combination of these (Marsay et al., 2014).

The CMIP5 models use either a sum of exponential or power-law expressions to represent the vertical flux of particulate organic matter (Fig. 6 and equations in Table A3) but do not yet capture the observed latitudinal variability (Fig. S2). In models where detritus is not represented explicitly, a large transfer of POC flux from upper layers to deeper layers is equivalent to a slow decrease of POC flux with depth and a low exponent in the Martin's power-law curve (Martin et al., 1987). Models with explicit detritus representation would replicate this effect by either using a sinking speed that is too high or a remineralization rate that is too low(see Table A3). For example, IPSL-CM5A-MR prescribes an approximate power law with a lower exponent (higher transfer efficiency) than HadGEM2-ES (Fig. 6c–d). Exponential curves would also create a large POC transfer from subsurface to intermediate depths as the curvature of the depth profile at 100–300 m is usually lower than for power-law profiles with exponents between 0.8 and 0.9 (typical profiles according to Martin et al., 1987). This low subsurface POC remineralization (large transfer) combined with a sudden increase in the POC remineralization (low transfer) at intermediate depths (300–800 m) results in stronger-than-observed remineralization in the low oxygen part of the column, forcing anomalous formation and extension of OMZs (for example, see the CESM1-BGC POC sinking profile in Fig. 6b). In conclusion, in order to match the observed oxygen concentrations, we propose that a Martin's exponent higher than typically observed values and a power law (instead of exponential) are preferable, as they ensure large remineralization rates in the upper layers and thus reduce anomalously high transfer of POC and oxygen consumption at depth. This agrees with findings from Kriest et al. (2010) based on sensitivity studies to the remineralization curve.

According to these expectations, the CMIP5 models with exponential profiles usually produce deeper oxygen consumption associated with respiration than the models that use a power law (Fig. 6 and Table A3). NorESM1-ME and MPI-ESM both show an exponential profile and show similarly deep OMZ (Fig. 6a). These models share the same biogeochemical module HAMOCC and differ in the representation of physical processes, suggesting that indeed their exponential parameterization of the remineralization curve is the cause for the deep OMZ. The GFDL-ESM2 models, with deep OMZs, also use an exponential profile (Fig. 6a).

In the subsurface, extensive denitrification worsens the problem of low-oxygen biases at depth. Models typically

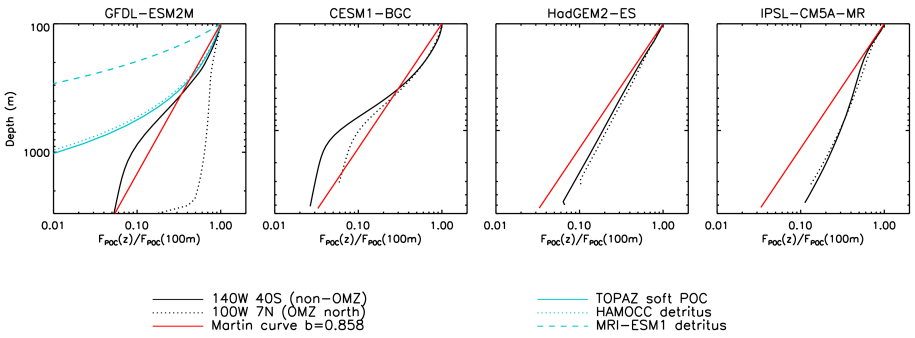

Figure 6. POC flux profile normalized to the value at 100m in the four CMIP5 models that provided three-dimensional data: **(a)** GFDL-ESM2M, **(b)** CESM1-BGC, **(c)** HadGEM2-ES, and **(d)** IPSL-CM5A-MR. The depth profile is shown for two locations, a typical non-OMZ region at 40° S (solid black) and a typical OMZ (dashed black). The red line in each panel is a power law with exponent 0.858 (Martin et al., 1987). Note that GFDL-ESM2M and CESM1-BGC POC flux profiles are modelled as exponential curves, while IPSL-CM5A-MR and HadGEM2-ES profiles are modelled as power laws (see equations in Table A3). In panel **(a)**, we also show the transfer efficiency for the exponential soft POC remineralization flux in TOPAZ2 (GFDL-ESM2 models), HAMOCC (NorESM1-ME and MPI-ESM models), and MRI-ESM1, all of them modelled as exponentials.

have an oxygen cut-off for respiration – discussed in Table A2 – below which denitrification remineralizes organic matter by consuming nitrate instead of oxygen. The length scale of remineralization is usually larger in denitrification than in oxic remineralization, pushing POC deeper in the water column and hence causing the OMZs to extend deeper than under oxic remineralization. Even though the remineralization length scale (and thus oxygen consumption) is similar between HAMOCC and TOPAZ (biogeochemical module for GFDL-ESM2 models) – 200 and 187.5 m, respectively – the length scale of denitrification is considerably larger in TOPAZ (1500 m) compared to HAMOCC (1000 m). This leads to POC being transported deeper in GFDL-ESM2 models compared to the NorESM1-ME and MPI-ESM models (also see Dunne et al., 2012). Additionally, the inclusion of ballast terms (Armstrong et al., 2002) in TOPAZ contributes to increase further the transfer of POC to deep waters.

The model CESM1-BGC does not develop a deep OMZ despite using an exponential curve (Fig. 6b, 2), similar remineralization parameters and ballast terms to GFDL-ESM2 models, partly because the denitrification length scale is much lower than in GFDL-ESM2 (260 m compared to 1500 m). Additionally, the CESM1-BGC model adjusts the nitrate consumed during denitrification to lower values to avoid running out of nitrate (Lindsay et al., 2014), such that the same amount of nitrate supports a larger POC remineralization. This fixes nitrate concentrations and decreases the transfer of POC to deeper waters, which might partially solve the expansion of OMZ.

MRI-ESM1, also with an exponential profile (Fig. 6a), does not develop deep OMZs, due to a very low transfer of POC to deep waters (large exponent in Table A3), which facilitates consumption in the upper ocean. Even though MRI-ESM1 thus solves the deep anoxia problem, the shallow modelled nitrate and POC export are higher than observed possibly due to recycling of organic matter near the surface that is too fast (Fig. 3c).

Only two models use a power law as a remineralization profile. The HadGEM2 models, with an exponent power law as in the Martin curve (Fig. 6c) and no denitrification, do not develop as deep an OMZ as expected. While in theory a power law is preferable to an exponential, the IPSL-CM5A models uses a very low exponent (relative to the Martin curve, Fig. 6d and. S2), resulting in a high transfer of POC to deep waters, which explains the positive oxygen anomalies in subsurface layers and contributes together with a lack of deep ventilation to a deep hypoxic region (Fig. 2).

Treatment of POC at the sea floor

If models bury a fraction of POC into the sediments when reaching the sea floor, the sensitivity of oxygen consumption to POC profile is reduced (Kriest and Oschlies, 2013). In the opposite case, if POC is remineralized back to the water column when hitting the floor, it could enlarge considerably the OMZ in models with high deep POC flux. NorESM1-ME and MPI-ESM are the only models that include a full sediment module such that part of the POC reaching sediments becomes unavailable to remineralization at each time step (Table A3). In IPSL-CM5A models, sinking organic matter is permanently buried below the sea floor, where it is not subject to remineralization. Hence, the low levels of oxygen in this model are more likely attributed to ventilation deficiencies. The rest of the models remineralize the remaining POC back to the water column when reaching the sea floor (Table A3).

The impacts of sediment scheme differences are most noticeable among models with low oxygen and high POC at depth. While the tropical OMZ reaches the bottom in GFDL-ESM2 models (consistent with no sediment scheme and in-

stant remineralization), the OMZ does not reach the bottom in the NorESM1-ME and MPI-ESM models (consistent with partial organic matter burial in sediments). We do not observe any impact of sediment scheme on the depth distribution of OMZs in other models.

3.1.3 Suggestions for improving the representation of OMZs in models

The ultimate question is what proportions of the excessive OMZ volume are due to equatorial zonal ventilation, mid-depth ventilation (from AAIW, SAMW and NPIW) and local consumption (remineralization), respectively. We agree with previous studies (Stramma et al., 2010a; Dietze and Loeptien, 2013; Montes et al., 2014) that an accurate description of local equatorial ventilation in the Pacific Ocean would help reduce the large modelled volume of OMZs by providing additional channels for the supply of oxygen-rich waters and the removal of low-oxygen and nutrient-loaded waters. This requires a very high resolution for improving the representation of all the equatorial jets or alternatively a parameterization of intermediate jets, for example by using anisotropic diffusion coefficients (Getzlaff and Dietze, 2013). Correct lateral ventilation from the Southern Ocean and North Pacific is also important for the correct characterization of OMZs, stressing the need to solve the insufficient flow of AAIW/SAMW and the often exaggerated deep North Pacific ventilation via NPIW or via AABW as discussed in Sect. 3.1.1 (Fig. 2). With more realistic equatorial ventilation, the depth of the OMZs would probably be less sensitive to slight changes in POC profiles, as most remineralization would happen in the upper ocean without the need to switch so extensively to denitrification, which in turn causes the OMZs to extend more deeply. On the other hand, reduction in the POC flux leaving the euphotic layer and a shallower remineralization achieved by using a power-law curve with low transfer of POC to deep waters, or a large denitrification rate, would improve the representation of the OMZs even before the representation of equatorial ventilation is improved. Additionally, the inclusion of a sediments module that does not prescribe instantaneous consumption of all the POC that reaches the sea floor but instead involves partial burial might alleviate the anomalously deep OMZ.

3.1.4 Overlap between observed and modelled OMZs

In order to evaluate the performance of CMIP5 models regarding their representation of OMZs in the tropical Pacific, we introduce a metric aimed at identifying the spatial overlap between observed and modelled OMZ (Fig. 7 and S3). The metric is calculated by finding, for a given oxygen threshold, the volume that results from the intersection of modelled and observed OMZ, and dividing it by the volume that results from the union of modelled and observed OMZs. A metric value equal to 1 means that modelled and observed OMZs occupy the same exact volume, while a value close or equal to 0 signifies a lack of intersection or/and a large difference in area extension between the modelled and observed OMZs. This metric penalizes models that misplace the OMZs compared to observations or models that enclose the observed OMZ area/volume but overestimate the OMZ extent.

Generally, the models are not capable of successfully representing anoxic zones ($O_2 < 10\,\mathrm{mmol\,m^{-3}}$), but show gradual improvement as O_2 concentration thresholds increase (Fig. 7a). As oxygen thresholds progressively increase from 10 to $100\,\mathrm{mmol\,m^{-3}}$, CESM1-BGC is always found to be closest to observations everywhere in the tropical Pacific (Fig. 7 and S3). While its overlap metric value is only 0.2 at $O_2 < 10\,\mathrm{mmol\,m^{-3}}$, it markedly improves to 0.7 when the threshold O_2 is set to $100\,\mathrm{mmol\,m^{-3}}$. Another model that is close to observations in the North Pacific is MPI-ESM (Fig. S3). In the South Pacific, both CESM1-BGC and MRI-ESM1 reproduce the observations fairly well, followed by HadGEM2 (Fig. S3). Importantly, in the surface layers (depth range from 0 to 400 m), most models perform similarly, reaching an overlap metric of about 0.6 at hypoxic concentrations ($O_2 < 60$–$80\,\mathrm{mmol\,m^{-3}}$), with the exception of IPSL-CM5A and HadGEM2-ES with substantially lower overlap metric values (Fig. S3). Panels (b) and (c) in Fig. 7 show in detail model performance at each depth when OMZs are defined with O_2 threshold of $50\,\mathrm{mmol\,m^{-3}}$. Panel (b) shows once more that some models predict OMZs to be too deep. Most models reproduce the depth at which the northern OMZ is largest, around 1000m, well despite the dispersion in OMZ area across models. However, in the Southern Hemisphere (SH), most models predict the largest OMZ to be deeper than observed. Most models achieve the best overlap metric at 300 m depth in the SH and 500 m depth in the Northern Hemisphere (NH) and progressively fail to reproduce the OMZs at shallower and deeper depths (Fig. 7c). Similar conclusions apply when other oxygen thresholds are considered.

3.2 Oxygen changes in the Pacific from 1990 to 2090

In this section we present changes in oxygen concentrations and the extent of OMZs in the Pacific throughout the 21st century, as well as the mechanisms responsible for those changes. We also explore how the biases found across CMIP5 models in the mean state (Sect. 3.1) propagate into 100-year timescale changes. Global changes in oxygen concentrations are summarized in Table 1 for all the CMIP5 models. Changes in O_2 can be due to either changes in AOU or changes in O_2sat:

$$\Delta O_2 = \Delta O_2\mathrm{sat} - \Delta \mathrm{AOU}. \quad (1)$$

We find that on average across all CMIP5 models, oxygen decreases around 3 % globally by the end of the 21st century (in agreement with Bopp et al., 2013). This drop is due to both global average decreases in O_2sat and increases in AOU, with

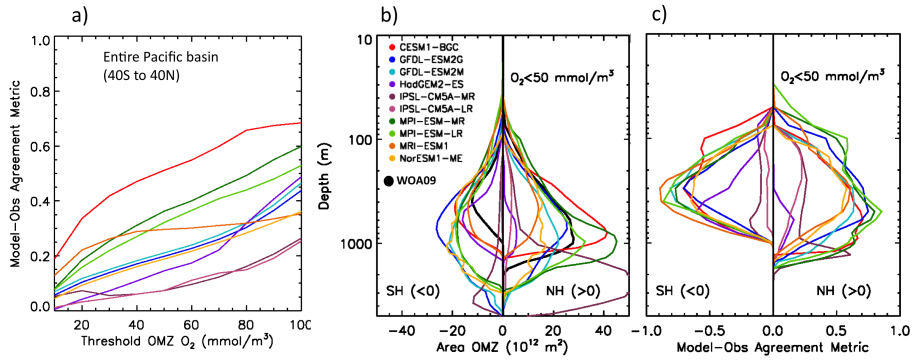

Figure 7. Agreement between modelled and observed OMZ extension in the Pacific during the historical period (1960–1999). **(a)** The agreement of modelled OMZs with observations is shown as the ocean volume that results from the intersection of the modelled and observed OMZs, divided by the volume that encompasses both modelled and observed OMZs. The OMZ volume is calculated at different O_2 thresholds (x axis). **(b)** Area of low-oxygen waters ($O_2 < 50\,\mathrm{mmol\,m^{-3}}$) at each depth across CMIP5 models and observations in the Southern Hemisphere (SH) (0–40° S; negative values) and in the Northern Hemisphere (0–40° N; > 0) as labelled. **(c)** Agreement of modelled OMZs with observations at each depth, shown separately for SH (0–40° S; < 0) and Northern Hemisphere (NH) (0–40° N; > 0). The agreement is calculated as in **(a)** and goes from 0 (no agreement) to 1 (perfect agreement). The model HadGEM2-CC (not shown) shows results similar to HadGEM2-ES.

similar contributions from each in the multi-model mean (Table 1). The drop in oxygen originally stems from high latitudes and deep oceans (Fig. 8c), and is due to a combination of O_2sat decreases (Fig. 8f) and AOU increases (Fig. 8i). As expected, the thermal contribution (via ΔO_2sat) to the global oxygen decrease (ΔO_2) was lower, around 25–50 %, in the previous Coupled Model Intercomparison (CMIP3) under the SRESA2 scenario (with less overall warming than RCP8.5), while the rest was ascribed to changes in oceanic ventilation (e.g. Table 2 in Keeling et al., 2010). Historical measurements from the 1970s to the 1990s already reflect these long-term predictions (Helm et al., 2011).

Next we discuss centennial changes in oxygen across different regions. In Fig. 8 we show a meridional section of the eastern Pacific for O_2, O_2sat, AOU, and water-mass age . The historical observed values together with the historical multi-model averages are shown in Fig. 8 in reference to Sect. 3.1. The last column of Fig. 8 shows the multi-model averaged centennial changes and the consistency of the predicted trends across models (for individual model projections see Figs. S4, S5, and S6). Figure 10a (described later) shows a schematic of the regions of interest described in the following text.

Zones of subduction and propagation of deep water masses

Surface freshening and warming south of 60° S were shown to result in a weakening of AABW formation over the 21st century for IPCC AR4 models (Sen Gupta et al., 2009). Additionally, warming and freshening in the formation zones of mode and intermediate water masses (Sallee et al., 2013a) result in a reduced ventilation of Southern Ocean intermediate layers across CMIP5 models under the RCP8.5 scenario (Sallee et al., 2013b), as also observed by Downes et al. (2010) across IPCC AR4 models under the SRESA2 emissions scenario. Meijers et al. (2014) provide a complete review of the transformation of water masses under climate change across CMIP5 models.

The usual expectation is that for a given water mass, the older the age, the more time there is for organic matter and oxygen to be consumed, hence the higher the AOU, and the lower the O_2 in the water sample. This relationship holds well over most of the deep ocean on interannual timescales, as seen by the positive correlation between age and AOU in Fig. S7a and the negative correlation between AOU and O_2 in Fig. S7b. This relationship also holds well on centennial timescales. We see that, over the 21st century, climate-driven decreases in deep ocean ventilation along the AABW in the Southern Ocean and along the NPIW in the North Pacific increase age (Fig. 8l) and increase AOU (Fig. 8i), contributing to a decrease in O_2 along these ventilation pathways (Fig. 8c). The patterns of increased AOU and decreased oxygen can also be seen in individual model projections (Fig. S4 and S5).

However, the expected relationship between water-mass age and AOU is opposite from expectations in the deep North Pacific in the NorESM1-ME and GFDL-ESM2G models, i.e. decreased ventilation (Fig. S6) is accompanied by decreased AOU (Fig. S5). Interestingly, the same mechanism that controls the relation between age and AOU interannually controls the 100-year time changes in the four models that include age tracers (not shown). The deep North Pacific is the least ventilated basin, such that isopycnal ventilation is weak there and the diapycnal supply of oxygen gains importance (Karstensen et al., 2008), which could contribute to the age–AOU disagreement. Moreover, with climate change, the per-

Table 1. Long-term trends in global oxygen and contribution from O_2sat and AOU across CMIP5 models (columns). The first row shows global oxygen during the historical period 1960–1999, the second row shows relative change over 100 years from 1960–1999 to 2060–2099 (in %), and the third and fourth rows show the percentage of oxygen decrease due to a decrease in O_2sat and an increase in AOU. The last column shows the multi-model average and standard deviation (SD) by weighting models as described in Table A1.

	CESM1-BGC	GFDL-ESM2G	GFDL-ESM2M	HadGEM2-ES (CC)	IPSL-CM5A-MR (LR)	MPI-ESM-MR (LR)	MRI-ESM1	NorESM1-ME	Multi-model Average (SD)
O_2 (mmol)	190.9	188.3	171.8	178.1 (177.0)	137.0 (148.4)	174.5 (176.1)	209.8	236.3 (26.0)	186.6
$\Delta O_2/O_2$ (%)	−3.1	−2.7	−3.5	−3.9 (−3.7)	−3.6 (−4.0)	−2.5 (−2.8)	−1.3	−1.3 (0.9)	−2.8
ΔO_2sat/ΔO_2 (%)	41.3	44.4	40.0	34.2 (33.5)	46.0 (38.0)	52.6 (49.7)	54.5	88.2 (15.9)	49.4
$-\Delta$AOU/ΔO_2 (%)	58.7	55.6	60.0	65.8 (66.5)	54.0 (62.0)	47.4 (50.3)	45.5	11.8 (15.9)	50.6

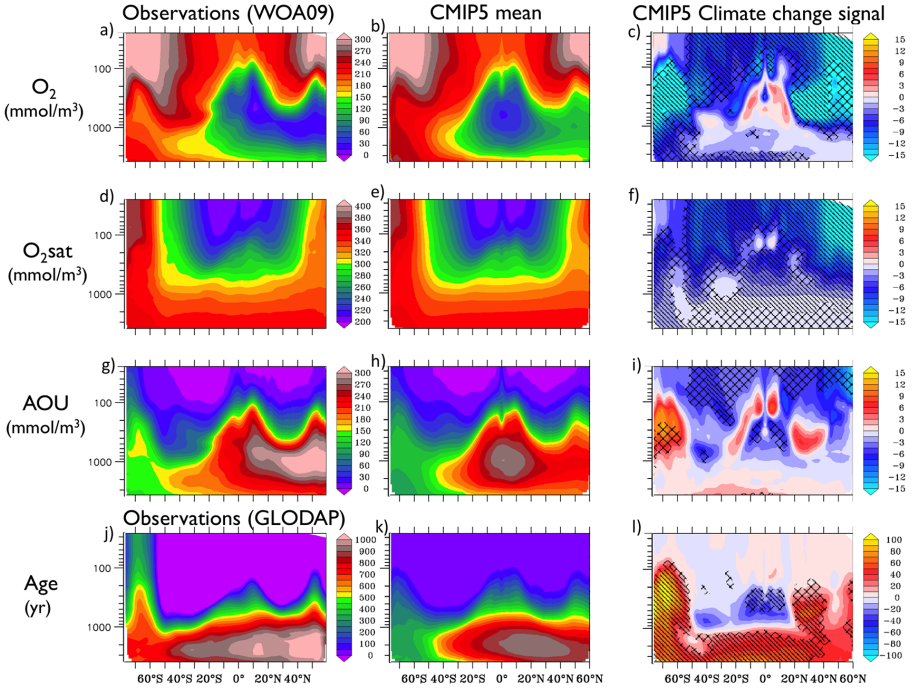

Figure 8. Observational climatologies from WOA09 and GLODAP data sets (left column), CMIP5 multi-model mean historical simulations for the period 1960–1999 (middle column) and CMIP5 multi-model mean future projections for the period 2060–2099 referenced to the historical period (right column) for oxygen concentration (mmol m^{-3}) on the first row, O_2sat (mmol m^{-3}) on the second, AOU (mmol m^{-3}) on the third, and water-mass age (yr) on the last row, all averaged zonally between 180° W and 100° W for a number of depths (y axis shows depth in m). The predicted 100-year change panels include diagonal pattern for trends that are consistent across CMIP5 models at the 90 % level, and crossed patterns for 80 % level. The observed age was multiplied by 2 in order to match the CMIP5 magnitude qualitatively. Only four of the studied models reported age. The metrics for 100-year change agreement is explained in the Methods section.

centage of saturated O_2 could increase, which then would increase the input of oxygen into the ocean interior, ultimately decreasing the estimated AOU (that assumes O_2 to be 100 % saturated at the surface) even if respiration increased (Bernardello et al., 2014). As a result of decreased AOU in the North Pacific, AOU does not increase as much globally in NorESM1-ME compared to other models. Therefore, this model experiences a lower decrease in global O_2 (1.3 %) over the 21st century, mostly driven by the contribution of O_2sat decrease (82 % in Table 1) with little contribution from AOU increase, contrary to the rest of models (Table 1).

O_2sat decreases in zones of deep water-mass formation (Fig. 8f) due to 21st century warming, contributing (together with the increase in AOU) to the decrease in oxygen levels in deep waters. Note that AOU and O_2sat are anti-correlated in zones of deep water subduction on both centennial and interannual scales as decreased ventilation (and hence increased AOU) is usually associated with warmer waters (and lower O_2sat; Fig. S7d).

Upper ocean (top 100 m)

In the upper ocean above the thermocline, O_2sat drops significantly everywhere as temperature increases (Fig. 8f), acting to decrease O_2 (Fig. 8c). O_2sat dominates the changes in O_2 on both the 100-year timescale and the interannual scales (Fig. S7c). The exception to this are the low-oxygen subsurface eastern zones where O_2 is predicted to increase over the 21st century following a strong decrease in local AOU, higher than the warming-induced decrease in O_2sat.

This decrease in AOU results from both a strong stratification-driven decrease in nutrient supply and reduced mixing with old high-AOU waters under future warming.

Low-latitude intermediate depths (200–1000 m)

At low-latitude intermediate depths, the changes in oxygen levels over the 21st century are small in the multi-model mean (Fig. 8c), owing to a strong compensation between decreased AOU and decreased O_2sat (reduced solubility). The decreasing trends in both AOU and O_2sat are consistent across models in the most central part of this region (Fig. 8f and i). Increased stratification reduces the supply of nutrients to the euphotic zone, acting to reduce productivity and consumption of oxygen (AOU decrease) especially in the eastern highly productive tropics. However, changes in ventilation (as tracked by the water-mass age) explain most of the decrease in AOU outside the eastern anoxic regions (Fig. 8l). Both water-mass age and AOU drop due to a decrease in the upward transport of old, high AOU deep waters (Fig. 8h, k) following increased stratification (Gnanadesikan et al., 2007, 2012). The oxygen trend is highly inconsistent across models, as seen in Fig. 8c (no patterns). Inter-model discrepancies in predicted trends result from the strong compensation between decreased O_2sat and increased AOU and from slight differences across models in the exact location of this poorly ventilated region (Fig. S4). The finding that the multi-model mean change in O_2 is not significant agrees with previous model studies (Cocco et al., 2013; Bopp et al., 2013 across CMIP5 models).

As oxygen remains approximately constant with climate warming in mid-depth tropics, 21st century changes in tropical OMZ volume are small in most CMIP5 models (Fig. 9 and S8). In anoxic regions ($O_2 < 5\,\mathrm{mmol\,m^{-3}}$) CMIP5 models show an increase or decrease in volume (by about 10 %) depending on the balance between O_2sat and AOU contributions and changes are indistinguishable from natural variability for GFDL models. Changes in the volume of anoxic regions are of critical importance for the survival of organisms and for denitrification, which occurs at low oxygen values. However, the skill of models in representing anoxic regions is poor (Fig. 7a), so this result should be taken with caution. The volumes of hypoxic regions ($O_2 < 80\,\mathrm{mmol\,m^{-3}}$) mostly increase, although slightly, due to decreased overall ventilation and increased AOU. Hypoxic volumes encapsulate

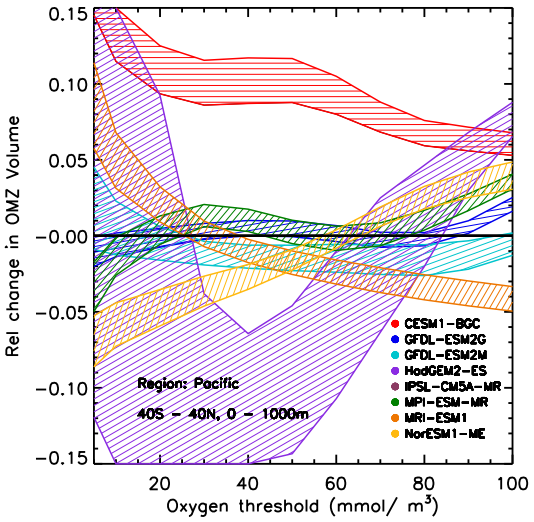

Figure 9. Relative change in the volume of oxygen minimum zones in the Pacific between 40° S and 40° N latitude to 1000m depth over 100 years (from the period 1960–1999 to the period 2060–2099) projected by individual CMIP5 models. Each model projection is shown as a patterned band that encompasses the natural variability (mean 100-year change ±1 standard deviation over 40 years in the control sample). MPI-ESM-LR and HadGEM2-CC are not shown for clarity, as these are very similar to MPI-ESM-MR and HadGEM2-ES. IPSL-CM5A-MR model lies outside of the plot limits and is shown in Fig. 7.

wider regions than anoxic regions, so these are not dominated anymore by local consumption but by overall ventilation. As an exception, IPSL-CM5A predicts an increase of both anoxia and hypoxia (this model can only be seen in Fig. S8), as changes in oxygen levels are dominated by decreased ventilation even within anoxic regions. CESM1-BGC similarly predicts an increase in OMZ volume everywhere, driven by changes in ventilation at intermediate depths (500–1000 m). The anomalously high interannual variability in HadGEM2 in anoxic regions is due to a small OMZ size, which artificially boosts the relative changes.

Summary

In accordance with the regimes just explained, we identify three zones in the Pacific Ocean with similar properties: (i) surface layers, (ii) deep Pacific and high-latitude intermediate depths (coinciding with the multi-model increase in age in Fig. 8l), and (iii) low-latitude intermediate depths (coinciding with the multi-model decrease in age in Fig. 8l). Figure 10 shows trends in O_2, O_2sat, and AOU across CMIP5 models separated into (a) a surface box (50 to 200 m), (b) an intermediate box (200 to 1000 m), and (c) a deep box (2000 to 4000 m). Surface O_2 is predicted to decrease in all the models due to warming-driven O_2sat decrease (Fig. 10a). In the deep Pacific, most models show a decrease in oxygen levels, due to reduced ventilation (increased water-mass

age) – increase in AOU – and due to increased temperature – decrease in O_2sat (Fig. 10c). Similarly, high-latitude intermediate depths (between 200 m and 1000 m) in the zones of water-mass formation are expected to experience decreases in oxygen concentrations (shown in blue in Fig. 10b) due to decreased ventilation, as in the deep box, coinciding with the multi-model increase in age in Fig. 8 l. Only at the low-latitude intermediate depths (OMZ region, red in Fig. 10b), where AOU mostly decreases due to reduced mixing with old waters, are oxygen levels predicted to remain nearly constant (i.e. to increase or decrease only slightly, depending on the model) due to a high degree of compensation between changes in O_2sat and AOU (Fig. 10b). Importantly, the same physical regions can be analysed on interannual timescales (Fig. S7). Surface oxygen is dominated by changes in O_2sat (Fig. S7b) and oxygen at deep and high latitudes is dominated by changes in AOU (Fig. S7b) which is in turn very correlated to changes in age (Fig. S7a). Low-latitude intermediate oxygen changes result from a compensation between increased O_2sat and decreased AOU (or opposite) as seen in Fig. S7d and discussed in the next section.

It is worth noting that we found no correlation between biases in the mean state and responses to climate change, suggesting that the mechanisms underlying the change are similar and robust in all models.

3.3 Oxygen dynamics in the eastern tropical Pacific OMZ: interannual variability compared to long-term changes

The most interesting dynamic in the oxygen system is the strong compensation between AOU and O_2sat through the 21st century below the thermocline in the eastern tropical Pacific (Fig. 8c, f, i). In this section we highlight the mechanisms controlling oxygen variations on both interannual and long-term timescales between 10° S and 10° N and east of 115° W, at a depth of 100 to 200 m. This domain is chosen to enclose the upper portion of the eastern tropical Pacific OMZ, found to have interesting oxygen dynamics due to the strong compensation between AOU and O_2sat through the 21st century (Sect. 3.2, Fig. 8c, f, i). We explore here the same compensation mechanisms discussed in Sect. 3.2 but on interannual timescales. This region is also of interest because tropical oxygen is underestimated in many CMIP5 models compared to observations (Fig. 3a), since models do not properly separate the northern and southern OMZs (Fig. 1) as explained in Sect. 3.1.

The temporal evolution of the system is shown in Fig. 11 both for interannual variability (ellipses) and for long-time trends (wiggly lines) across CMIP5 models. For each model, the ellipses encapsulate 95 % of the interannual variability calculated in the 100-year control time series.

On interannual scales, the oxygen concentration in this eastern Pacific region depends on the compensating effects between increased O_2sat and increased AOU (Fig. 11a),

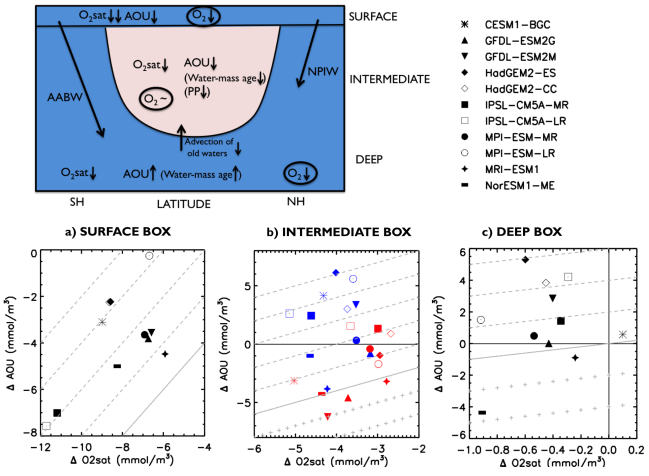

Figure 10. Top: schematic of the 100-year change (1960–1999 to 2060–2099) in O_2 across CMIP5 models. Bottom: relationship between the 100-year change in apparent oxygen utilization (ΔAOU, mmol m^{-3}) and the analogous change in O_2sat (ΔO_2sat, mmol m^{-3}) estimated by individual CMIP5 models in the Pacific Ocean in **(a)** the surface layer (average from 50 m to 200 m), **(b)** the intermediate layer (average from 200 to 1000 m) and **(c)** the deep layer (average from 2000 to 4000 m). Solid grey lines in panels indicate no change in oxygen, dashed lines indicate decrease in oxygen concentration (–), and plus lines indicate increase in oxygen (+). In the intermediate box, low-latitude values are represented in red (coinciding with decrease in multi-model mean age of at least 20 years) and high latitudes, i.e. zones of water formation (where age increases), are shown in blue.

which are highly correlated since both are forced by changes in the Walker circulation (Fig. 11b–c). During years with strong upwelling (coinciding with "La Niña" events or a strong Walker circulation) the thermocline shallows in the East Pacific. An increased zonal tilting of isopycnals brings more nutrients to the surface increasing photosynthesis, local remineralization, and AOU, and acts to decrease O_2. Additionally, increased Walker circulation is also associated to increased inflow of deep water, which is not well ventilated and thus contains high levels of accumulated AOU, also acting to decrease O_2 in the OMZ region. At the same time, the upwelling of cold deep waters results in a temperature-driven increase in oxygen solubility (O_2sat) and thus an increase of O_2.

On interannual scales, all the models predict O_2 changes dominated by AOU changes, shown by the slopes of the ellipses in the O_2sat–AOU relation in Fig. 11a. Hence, a strong Walker circulation results in increased O_2. The variability in O_2sat, controlled by physical mechanisms only, is more tightly related than AOU to changes in Walker circulation (less dispersion in ellipses in Fig.11b vs. 11c) at all depths. A more detailed analysis shows that changes in AOU are due to local remineralization at 100 m but become gradually more dominated by changes in water-mass age at 200 m and be-

low. These considerations apply to the whole suite of CMIP5 models, and support results from the hindcast model by Ito and Deutsch (2013). It is worth noting that most models overestimate O_2sat compared to observations (cross in Fig. 11) due to the well-known cold bias in the tropics (Li and Xie, 2014). AOU is also overestimated in seven models, because of the nutrient-trapping problem discussed in Sect. 3.1.2. However, the strength of the modelled Walker circulation and its natural variability is similar to the observed one (Fig. 2b–c) except for GFDL-ESM2M, which overestimates Walker circulation variability.

The centennial behaviour is illustrated by the AOU, O_2sat, Walker, and stratification index trajectories from 1900 to 2099 (wiggly solid line in Fig. 11a–e). The 100-year trend in Walker circulation strength is low and discrepant across the CMIP5 ensemble (Fig. 11b wiggly lines), although most models show a slight decrease of its strength (Sandeep et al., 2014 and reference therein). However, the eastern tropical Pacific in CMIP5 models stratifies, mainly due to increased warming and increased precipitation (Cabré et al., 2015) and not due to centennial changes in Walker circulation strength. As a consequence, fewer cold, old and nutrient-rich waters are upwelled and mixed from deeper layers as explained in Sect. 3.2. The consequent decrease in surface productivity and in water age results in less local and accumulated oxygen consumption via remineralization (less AOU) across all models (Fig. 11d). Additionally, O_2sat gradually decreases across all models as a result of reduced inflow of cold, deep waters and an overall increase in ocean temperatures (Fig. 11e). Note that while we define stratification here as the density difference between 200 m and surface, the analysis of other variables, depicting changes in density structure such as thermocline depth, shows similar results.

The centennial behaviour of the system (wiggly lines) is different from the interannual variability (ellipses). Although the sensitivity to changes in stratification for O_2sat is the same for interannual and 100-year timescale (Fig. 11e ellipse slope similar to 100-year trend slope), the sensitivity to changes in stratification for AOU is larger for interannual compared to the centennial timescale (Fig. 11d ellipse slope larger than 100-year trend slope). As a result, the reduction of O_2sat relative to the reduction in AOU is more pronounced on the 100-year timescale than on the interannual timescales (Fig. 11a). Graphically, this means that the O_2 centennial wiggly line in Fig. 11a becomes more parallel to the constant O_2 lines compared to the ellipse slope. Thus, on the 100-year timescale there is almost perfect compensation between the AOU and O_2sat, such that O_2 does not change significantly across the CMIP5 models. By contrast, AOU changes dominate O_2sat changes, resulting in more significant changes in O_2 on the interannual timescales. We hypothesize that this differential behaviour on different timescales is due to the fact that increased stratification with climate change moves the isopycnals deeper, changing the relative importance of lateral over vertical mixing. Moreover, we hypothesize that the local biological positive feedback, very important at interannual scales for AOU changes, is dampened at longer timescales as the system adjusts the new levels of physical nutrient supply.

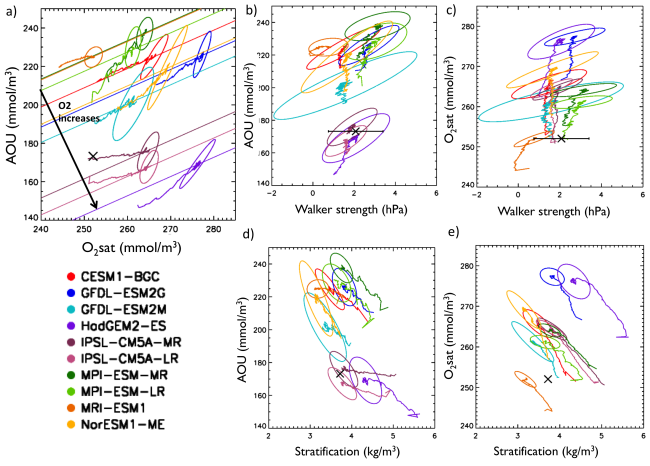

Figure 11. Interannual variability and climate-change trend in oxygen, AOU, and O_2sat for each CMIP5 model (symbolized by colours explained in the legend) in the eastern Pacific (from 10° S to 10° N latitude and 115 to 60° W longitude) at a depth of 100 to 200 m. Solid lines denote constant oxygen values ($O_2 = O_2$sat–AOU) at the pre-industrial concentration. Each ellipse encompasses 95 % of the interannual variability in O_2sat (x axis) and AOU (y axis), calculated in a 100-year period of the control run **(a)**. The wiggly line shows the 20-year smoothed climate change evolution from 1900 to 2099, starting from the centre of the ellipse and moving out of it as time passes. Observations are shown as a cross (WOA09). Subsequent panels show the effect of the Walker circulation strength on AOU **(b)** and O_2sat **(c)**, and the effect of stratification on AOU **(d)** and O_2sat **(e)**. Observed variability in Walker circulation is included in panels (b) and (c) (black line). The model HadGEM2-CC (not shown) shows results similar to HadGEM2-ES.

4 Conclusions

Here we studied the differences in contemporary and 21st century oxygen distributions across the latest generation of Earth system models CMIP5 in the Pacific Ocean. The range of physical and biogeochemical characteristics across CMIP5 models offers a unique opportunity to understand common and persistent mechanisms and biases.

We find that the volume of OMZs is systematically overestimated across CMIP5 models in agreement with previous work (e.g. Bopp et al., 2013), largely because of overestimated weakening of the Equatorial Undercurrent on the Eastern side, too weak surface countercurrents, and lack or deficiency of deeper equatorial jets. The biases in equatorial ventilation combined with large biological consumption result in strong oxygen depletion, phosphate trapping at depth, and nitrate that is (often) too low due to excessive denitrifi-

cation (Fig. 3). Consequently, most models tend to join the northern and southern OMZ cells – well separated in observations – into a single large tropical OMZ (Fig. 1a).

The southern Pacific OMZs are found to be too large compared to observations, as intermediate water ventilation from the Southern Ocean does not reach sufficiently north in the Pacific (in agreement with Sallee et al., 2013b and Downes et al., 2010). Some models additionally predict positive biases in oxygen concentrations at the northward edge of the northern OMZ, due to excessive NPIW transport and excessive deep ventilation from AABW towards the North Pacific. This creates a meridional distribution of oxygen that is too symmetric across the equator compared to observations (Fig. 1).

The POC flux at 100 m is significantly larger than observations across at least four CMIP5 models, triggering excessive oxygen consumption. The OMZ expands too deep for models with low remineralization in the upper ocean, associated with a high transfer of POC to deep waters. We find that a power-law POC remineralization profile with large shallow remineralization and low transfer of POC to the deep matches the observed oxygen concentrations better.

With realistic equatorial ventilation, the depth of the OMZ would probably be less sensitive to changes in POC profiles because it would not switch from aerobic remineralization to denitrification so easily, but until the representation of equatorial ventilation is improved, a higher exponent in the POC transfer power-law curve, and higher denitrification rates might alleviate the anomalously deep OMZ. We recommend the calibration and examination of sediment models, since the lack of sediment burial at the sea floor might contribute to anomalously deep OMZ if all the remaining POC is remineralized instantaneously at the sea floor.

Complexity in the representation of biogeochemistry does not seem an advantage in modelling OMZs within this generation of coarse-resolution simulations. The most complex biogeochemical models (CESM1-BGC, GFDL-ESM2, and IPSL-CM5A), with ballast- or size-dependent remineralization and denitrification, display OMZ biases similar to the rest of the models. We provide summary tables of ocean physics (Table A2) and biological representations and parameters (Table A3) for all the CMIP5 models analysed. These tables complemented with recommendations in Sect. 3.1.3 will be useful for modellers who want to improve the representation of OMZs, and the processes that control them. Furthermore, we created the overlap metric described in Sect. 3.1.4 to help select models with the least OMZ biases compared to observations for biogeochemical studies.

Under typical climate-change scenarios, all CMIP5 models predict similar deoxygenation mechanisms during the 21st century, despite large differences in the oxygen mean state. The consistency with which the different models predict changes in O_2sat and AOU suggests that the mechanisms underlying the change are similar and robust across all models and that biases in the mean state do not affect the expected response to climate change.

CMIP5 models predict a decrease of oxygen over most of the deep and high- latitude ocean due to an overall slowdown of ventilation (increased AOU) and increased temperature (increased O_2sat), in agreement with observed decreasing trends in deep O_2 over recent decades (Helm et al., 2011). Consistency among model predictions (Fig. 8c) and agreement with recent observed trends at high latitudes suggests that this is a robust mechanism that we should continue to monitor with future biogeochemical observing systems. We also find coherent patterns of oxygen trends with climate change in the Pacific surface (Sect. 3.2, Fig. 10a), where oxygen decreases due to warming (O_2sat decrease).

The most complex behaviour is displayed in the intermediate tropical depths where the OMZs reside. On interannual timescales, we find that both changes in O_2sat and AOU are systematically connected to the Walker circulation and ENSO variability across all CMIP5 models, as previously observed in the southern tropical Pacific (Llanillo et al., 2013) and discussed in a single hindcast model by Ito and Deutsch (2013). The interannual variability of the upper part of the tropical Pacific OMZ is dominated by changes in AOU over changes in O_2sat, such that years with strong Walker circulation are years of increased AOU and lower total oxygen.

In contrast to interannual variability, CMIP5 models project AOU increases and O_2sat decreases that almost compensate over the 21st century, such that climate-driven predictions in tropical mid-depth oxygen are consistent with no oxygen change across the CMIP5 models. This agrees with predictions from previous modelling studies (Bopp et al., 2002, 2013; Matear and Hirst, 2003; Cocco et al., 2013). The projected AOU decreases in the eastern tropical mid-depths throughout the 21st century are due to increased stratification and hence (a) less advection of deep, AOU-rich waters and (b) decreases in biological production; the projected O_2sat decreases are due to warming.

However, observations have shown a clear expansion of hypoxia in the tropics (Stramma et al., 2008, 2010a, 2012) over recent decades, contradicting the long-term predictions from models. Biases in the modelling of lateral ventilation via deep equatorial jets have been suggested as possible causes for discrepancy in predictions compared to observations (Stramma et al., 2010b; Getzlaff and Dietze, 2013), which could be too dominated by changes in vertical ventilation. It is also possible that the observed OMZ expansion in the tropics is mostly the result of natural variability on multi-decadal timescales, for example driven by changes in trade winds associated with the Pacific Decadal Oscillation (Deutsch et al., 2011, 2014; Czeschel et al., 2012). Trade winds regulate the strength of the subtropical–tropical cells (eg. Lübbecke et al., 2008), which modify the amount of oxygen transferred from the gyres to the eastern Pacific Ocean (Duteil et al., 2014b).

Appendix A: Model-by-model analysis of physical and biological processes contributing to biases in the Pacific oxygen minimum zones

All the CMIP5 models underestimate the equatorial ventilation, contributing to the anomalous merging of the northern and southern OMZs in the Pacific Ocean. Here, we describe in detail additional sources of bias, such as the ventilation from the Southern and North Pacific oceans and the parameterization of the remineralization profiles, which differ from model to model. The following results are based on Tables A1, A2, and A3 and references therein.

GFDL-ESM2M and GFDL-ESM2G

Biases

Both GFDL-ESM2 models display a large tropical OMZ, overestimate the southward extension of the southern OMZ, and underestimate the northward extension of the northern OMZ, which results in too much hemispheric symmetry in OMZs (Fig. 1). Both models overestimate the vertical depth of the OMZ (Fig. 1), despite large oxygen concentrations in the deep Pacific for GFDL-ESM2G (Fig. 2).

Mechanisms

Both GFDL-ESM2 models are biased towards low Southern Ocean intermediate ventilation and high North Pacific ventilation (NPIW), resulting in too much hemispheric symmetry in OMZs. The version ESM2M captures best the tropics, Southern Hemisphere, and deep Pacific oxygen, while ESM2G captures best the NPIW ventilation and consequently the northern OMZ. The excess in deep oxygen concentration in GFDL-ESM2G is related to large AABW formation rates.

Both GFDL models overestimate the extension and depth of OMZ, possibly due to equatorial under-ventilation that leads to nutrient trapping, and worsened by an excess of denitrification (also suggested by Dunne et al., 2012) and by the use of an exponential remineralization curve (Fig. 6). The OMZ shape is almost constant at different depths contrary to observations, suggesting that the OMZ is indeed maintained by a vertical mechanism as it would be too much POC flux and remineralization at depth. The denitrification length is considerably high in GFDL-ESM2 (1500 m), displacing POC remineralization and the OMZ deeper in GFDL-ESM2 compared to other models. Instantaneous remineralization of POC at the bottom floor (without burial of POC to the sediments) might also contribute to a OMZ that is too deep.

CESM1-BGC

Biases

CESM1-BGC represents the overall patterns in oxygen well, but overestimates the spatial extent of OMZ in the equatorial Pacific (Fig. 1). CESM1-BGC displays extended negative oxygen bias over most of the ocean (Moore et al., 2013). However, the NH OMZ matches the depth and patterns of the observed OMZ better than most CMIP5 models (Sect. 3.1.4).

A1 Mechanisms

A poor equatorial ventilation system, combined with underestimated mid-depth ventilation from the Southern Ocean and North Pacific results in an OMZ that is larger than observed.

The exponential curve used to represent soft POC is a potential source of bias that could be improved by applying a power law instead (Moore et al., 2013). Even though the remineralization curve is exponential and similar to the models that develop a deep OMZ (compare GFDL-ESM2 and CESM1-BGC remineralization curves in Fig. 6), CESM1-BGC does not develop such strong denitrification or deep OMZ. The denitrification rate is higher than in the other models with exponential profile (denitrification length equal to 260m instead of 1500m in GFDL-ESM2), alleviating the POC displacement to deeper depths. Additionally, the consumption of nitrate in denitrification is corrected to avoid a complete depletion of nitrate (Lindsay et al., 2014), possibly correcting for deep OMZ.

IPSL-CM5A-MR (LR)

Biases

This model forms a large OMZ in the deep North Pacific and shows low oxygen concentrations in the entire deep Pacific. However, the tropical mid-depth OMZ barely develops (mid-depth oxygen is too high compared to observations).

Mechanisms

The relatively low exponent in the power-law remineralization curve (Fig. 6 and Table 3) creates an extended deep OMZ (as also suggested by Dufresne et al., 2013) because it transfers too much POC to deep waters, shifting the OMZ to deeper depths and resulting in positive oxygen anomalies in the upper layers. The underestimate of the OMZ volumes (high levels of oxygen compared to observations) in the tropics and SH is also related to the fact that nutrients (and hence production) are underestimated there (Fig. 2, 3), probably due to weak EUC (Fig. 4). At the sea floor, all the remaining POC is buried into the sediments, a mechanism which prevents further hypoxia in the bottom layers.

MPI-ESM-MR (LR)

Biases

The tropical OMZs are too deep (as previously noted by Ilyina et al., 2013), too large, and expand too far poleward in both hemispheres. However, the oxygen concentration is overestimated in the deep Southern Ocean.

Mechanisms

Intermediate water masses are well represented in this model. However, AABW formation is underestimated, which might explain the large oxygen bias in deep low latitudes and the NH. Figure 4 shows the large bias in equatorial ventilation in the low-resolution version of the model (MPI-ESM-LR), which is much improved in the high-resolution version (MPI-ESM-MR). However, both resolution model versions show similar biases in oxygen distribution and an OMZ that is too deep, suggesting that the deep OMZ is mostly due to extra-equatorial ventilation or biological bias.

The modelled deep OMZ might result from an exponential remineralization curve with a low exponent (exaggerated with low denitrification rates and complete depletion of nitrate), combined with an overestimate of the POC flux from the euphotic layer (Fig. 5). The OMZ forms at a shallower depth than in other models and observations due to large POC flux in the euphotic layer.

NorESM1-ME

Biases

The oxygen in this model is too high in the entire deep Pacific and in the NH intermediate depths. However, the model develops large and deep OMZs in the tropical mid depths (Figs. 1, 2).

Mechanisms

The level of oxygen is too high everywhere surrounding the OMZs due to excessive deep-water formation that expands to the NH, and likely also enhanced by excessive NPIW mixing.

The OMZ is similarly deep in NorESM1-ME and MPI-ESM models. Both model groups share the same biogeochemical model HAMOCC (and very similar parameters) but differ in physics, suggesting that the remineralization curve is the cause for the deep OMZ extension. An exponential curve for remineralization profile transfers too much POC to deep waters, creating a deep OMZ in the Nor-ESM1 model (similar to GFDL-ESM2 and MPI-ESM models). The POC flux at 100 m is too large as shown in Fig. 5, contributing to the deep OMZ.

HadGEM2-ES (CC)

Biases

These two models form a large and deep southern OMZ that expands towards the tropics. However, no northern OMZ is formed, resulting in a positive oxygen anomaly compared to observations.

Mechanisms

According to Williams et al. (2014), the globally prevalent positive oxygen bias in HadGEM2-ES between 100 and 1000 m at low northern latitudes can be attributed to the underestimation of primary productivity at mid to high latitudes (and subsequent low consumption in the subsurface). We think that a strong NPIW also contributes to elevated oxygen advection and to the removal of the northern OMZ. In the southern Pacific Ocean, there is generally good agreement between observed and simulated PP (primary production) and oxygen fields (Williams et al., 2014), although the OMZ is too large there, possibly due to the low exponent assumed in the power-law remineralization curve.

MRI-ESM1-ME

Biases

This model shows a larger southern OMZ than observed, and a smaller northern OMZ than observed. Additionally, oxygen concentration is overestimated at large depths.

Mechanisms

The amount of nitrate available in the eastern tropics and southern low latitudes (Fig. 3) is anomalously high, causing the POC flux to be high in these zones (Fig. 5). The EUC is weaker than observed so it should not be the cause for high levels of nitrate. In this case, high levels of nitrate could be explained by trapping on the eastern side due to anomalously shallow remineralization (resulting in remineralized new nitrate). In order to match observed oxygen, a high exponent is prescribed for the exponential remineralization curve (Fig. 5). In the NH, both nitrate and POC flux are low compared to observations, hence the high exponent in the remineralization curve does not allow the NH OMZ to extend as northward as seen in observations. Moreover, the large NPIW ventilation contributes to the removal of the northern OMZ.

Table A1. Summarized information across CMIP5 models. The table includes: spatial resolution in the ocean, ocean module, ecology subroutine, phytoplankton types, references, and weight applied in the multimodel averages (see Methods). The major differences between HadGEM2-ES and -CC are the inclusion of an interactive tropospheric chemistry component in -ES, and different vertical atmospheric resolution in -ES (L30) and -CC (L60). The only difference between IPSL-CM5A-LR and -MR is the atmospheric horizontal resolution, $1.9° \times 3.75°$ for -LR (low resolution) and $1.25° \times 2.5°$ for -MR (medium resolution).

Model	Resolution (depth levels, long/lat)	Ocean module	References: physics	Ecology module	References: biogeochemistry	Weight assigned in multi-model statistics
CESM1-BGC	60, 1.125/0.27–0.53	CCSM4	Gent et al. (2011), Danabasoglu et al. (2012), Weijer et al. (2012)	MET	Moore et al. (2004), Moore et al. (2006), Moore et al. (2013), Moore and Doney (2007) Lindsay et al. (2014)	1
GFDL-ESM2G	63, 1/0.3–1	GOLD	Dunne et al. (2012)	TOPAZ2	Dunne et al. (2013)	1
GFDL-ESM2M	50, 1/0.3–1	MOM4p1	Dunne et al. (2012)	TOPAZ2	Dunne et al. (2013)	1
HadGEM2-ES (CC)	40, 1/0.3–1	HadGEM2	Collins et al. (2011), Jones et al. (2011), Martin et al. (2011)	Diat-HadOCC (NPZD)	Palmer and Totterdell (2001)	0.5 (0.5)
IPSL-CM5A-MR (LR)	31, 2/0.5–2	NEMOv3.2	Dufresne et al. (2013)	PISCES (from HAMOCC5)	Aumont and Bopp (2006), Séférian et al. (2013)	0.5 (0.5)
MPI-ESM-MR (LR)	40, 0.4/0.4 (1.5/1.5)	MPIOM	Jungclaus et al. (2013), Giorgetta et al. (2013)	HAMOCC5.2 (NPZD)	Ilyina et al. (2013)	0.5 (0.5)
NorESM1-ME	53, 1/1.25	based on CCSM4 & MICOM	Bentsen et al. (2013), Iversen et al. (2013), Tjiputra et al. (2013)	HAMOCC5.1 (NPZD)	Assmann et al. (2010)	1
MRI-ESM1	51 1/0.5	OGCM	Yukimoto et al. (2011)	NPZD	Yukimoto et al. (2011)	1

Table A2. Description of ventilation sources across CMIP5 models, including North Pacific ventilation via NPIW, deep ventilation via AMOC and AABW, intermediate-depth South Pacific ventilation via AAIW and SAMW, and equatorial ventilation. The diapycnal mixing coefficient A_{redi} (collected from references in Table 1) is shown in parentheses in the first column. The AABW strength is calculated as the maximum value of the lower cell in the Indo-Pacific meridional stream function at 30° S. Fig. S9 shows the stream function across CMIP5 models. Italic entries show contributions from the present research; regular font shows literature compilation.

Model (A_{redi})	North Pacific ventilation	Deep ocean ventilation	South Pacific intermediate ventilation	Equatorial ventilation
CESM1-BGC ($800\,\text{m}\,\text{s}^{-12}$)	NPIW formation in the North Pacific is weaker than observed (Moore et al., 2013)	AABW transport is consistent with observations but on the weak side (Danabasoglu et al., 2012). AABW_30S = 5.2 Sv *This might add to NH OMZ being too large, resulting from low deep ventilation to the deep North Pacific.*	Intermediate-depth AAIW and SAMW water masses are found more equatorward and weaker than observations, probably related to the underestimation of MLD near the formation region (Danabasoglu et al., 2012) *The Southern Hemisphere OMZ is then too large.*	The subsurface ventilation via isopycnal mixing at low latitudes is weak, which contributes to negative biases in oxygen concentration (Moore et al., 2013). However, this version shows improvements in subsurface equatorial jets thanks to improved wind stress (usually underrepresented in low-resolution simulations). Still, the modelled wind and precipitation forcing is more N-S symmetric than the observed one. The depth and strength of EUC are well represented (Danabasoglu et al., 2012).
GFDL-ESM2G (M) ($600\,\text{m}\,\text{s}^{-12}$)	The North Pacific is overly ventilated by NPIW in ESM2M. ESM2G represents the lack of oxygen ventilation in the North Pacific better than ESM2M, though still at the high end compared to observations. (Dunne et al., 2013) *The poleward extension of the northern OMZ is underestimated.*	ESM2G is overly ventilated south of 60° S, such that bottom waters in ESM2G propagate further northward than in ESM2M, resulting in younger deep waters in ESM2G than in ESM2M (Dunne et al., 2013). AABW_30S = 18.8 (14.2) Sv *Larger AABW ventilation in ESM2G leads to higher levels of oxygen in the deep North Pacific.*	ESM2M reproduces the observed areas of SAMW in the Southern Ocean between 40° S and 50° S, while ESM2G underestimates the production of these waters. ESM2G exacerbates the ESM2M oxygen bias in the tropical and southern subtropical oceans and Southern Ocean north of 60° S (Dunne et al., 2013).	ESM2M lacks ventilation in the eastern equatorial Pacific, and ESM2G exacerbates this oxygen bias even more. ESM2M represents better the tropical west Pacific than ESM2G (Dunne et al., 2013), which leads to a better representation of the OMZ (*less expanded to the west*).
HadGEM2-ES (CC) ($500\,\text{m}\,\text{s}^{-12}$)	*We suggest that an overestimation of the extension of NPIW ventilation contributes to the removal of the northern OMZ.*	HadGEM2-ES has well-developed upper and lower circulatory cells which are analogous to the (upper) North Atlantic Deep Water (NADW) and (lower) Antarctic AABW systems observed (Williams et al., 2014). The AMOC is only slightly weaker than observed (Martin et al., 2011). AABW_30S = 12.3 (13.4) Sv	HadGEM2-ES subducts intermediate waters in regions of the water column that are clearly too stratified (Sallee et al., 2013b). *The SH OMZ is then too large because of poor intermediate ventilation.*	*EUC too weak towards the east (Fig. 4), resulting in underestimated transport of nitrate, low primary production, and low POC flux.*
IPSL-CM5A-MR (LR) ($1000\,\text{m}\,\text{s}^{-12}$)	*We suggest that NPIW expands too deep, which contributes to the overestimation of oxygen in the northern OMZ regions.*	AABW_30S = 15.3 (13.5) Sv *The strength of AABW is normal among CMIP5 models.*	No reported bias in AAIW or SAMW.	The model tends to underestimate the high surface nutrient concentrations that are associated with the strong equatorial Pacific upwelling on the eastern side (Dufresne et al., 2013). *This is due to deficient eastward EUC velocity (Fig. 4). As a consequence, local PP is underestimated, and so is the OMZ extension.*
MPI-ESM-MR (LR) ($1000\,\text{m}\,\text{s}^{-12}$)	*NPIW well represented.*	AABW_30S = 7.9 (6.5) Sv *Our calculated AABW in Pacific is among the lowest across CMIP5 models, which could contribute to a negative oxygen bias in the deep tropics and NH.*	This model represents mid-depth AAIW and SAMW fairly well (Fig. 4, Junclaus et al., 2013).	Introducing an "eddy-permitting" grid configuration (MPI-ESM-MR, 0.4° precision) in the ocean leads to improvements in the representation of the equatorial current systems (Junclaus et al., 2013). In particular, the position of the maximum and the tilt of the core of the equatorial undercurrent (EUC) with depth are well captured in the MPI-ESM-MR model.
NorESM1-ME	*NPIW is too deep and poleward compared to observations, which contributes to the removal of the northern OMZ.*	The AMOC strength is in the upper range among models contributing to phase 3 of the Climate Model Intercomparison Project (CMIP3) and well above observations. It is not clear what causes the vigorous AMOC intensity (Bentsen et al., 2013). AABW_30S = 21.9 Sv *This results in anomalously large oxygen concentration at large depth and too small NH OMZ.*	The model realistically simulates the structure of AAIW and SAMW from the Southern Ocean (Tjiputra et al., 2013). *However, these waters seem to have oxygen concentrations that are too low (Fig. 2).*	*EUC is well captured in this model (Fig. 4).*
MRI-ESM1	*NPIW is too deep and poleward compared to observations, which contributes to the removal of the northern OMZ.*	AABW_30S = 9.9 Sv *The strength of AABW is normal among CMIP5 models.*	*We hypothesize that AAIW waters are deficient in this model (based on Fig. 2).*	*EUC is too weak in this model (Fig. 4).*

Table A3. Description of biological parameters that might affect OMZ extension, including POC flux profile, denitrification, nitrogen fixation, and sediment burial across CMIP5 models, summarized from references in Table A1, and our analysis (see also Fig. S1). Most CMIP5 biogeochemical models use a constant rate of remineralization r combined with a constant sinking speed of POC or a sinking speed increasing with depth. In the case of linearly increasing sinking speed $w(z) = w_o + a \cdot z$ and the POC flux profile (F_{POC}) follows a classical Martin power-law curve $F_{\mathrm{POC}}(z) = F_{\mathrm{POC}}(z_0)(z/z_0)^{-b}$, with b equal to r/a. In the constant sinking speed case, the POC flux profile follows an exponential curve $F_{\mathrm{POC}}(z) = F_{\mathrm{POC}}\,(z_0)\exp(-b \cdot z)$, with b equal to r/w (Kriest and Oschlies, 2008). Some models with an exponential POC profile give the exponent in terms of remineralization length λ, equivalent to $1/b$. Italic entries show contributions from the present research; regular font shows literature compilation.

Model	POC flux	Denitrification	Nitrogen fixation	Sediment remineralization
CESM1-BGC	Ballast model (Armstrong et al., 2002) with two sinking classes: (a) a soft POC that remineralizes at a fixed length scale (l = 130 m) with temperature dependence, and constitutes > 90 % of the POC leaving the euphotic layer. (b) a class strongly associated with mineral ballast types (including lithogenic particles, biogenic silica, and calcium carbonate), with deeper remineralization lengths. $F_{\mathrm{POC}}(z)/\ F_{\mathrm{POC}}\ (z = z_0) = \exp(-(z - z_0)\ T_f^{\mathrm{POC}}/l)$ *Curve dominated by soft POC at mid-depths, and by ballast POC at depth (sum of exponentials with different exponents).* *POC flux at 100 m is more smoothly distributed than in the other models (Fig. S1), and it is large everywhere in the tropics, which could explain partially why OMZ expands so much to the west.*	Switch to denitrification at O_2 < 4 mmol m^{-3} (l_{denit} =260m), based on Van Mooy et al. (2002), but corrected to avoid artificially deep OMZ via nitrate run-out, by multiplying the fixed N removal rate by the simulated nitrate concentration, divided by a factor of 110 (Moore et al., 2013). *As the removal of nitrate necessary to degrade POC is artificially reduced, there is no nitrate run-out, such that POC remineralization can continue. Avoiding complete run-out of nitrate should partially fix OMZ.*	Diazotrophs fix dissolved N_2 (with iron limitation). In the Pacific, simulated export is driven by upwelling with less influence by N fixation. N fixation had a modest impact on the organic flux sinking into the OMZs (Moore and Doney, 2007)	All the remaining POC is remineralized instantaneously when reaching the sea floor.
TOPAZ2 (GFDL-ESM2G, GFDL-ESM2M	Ballast model (Armstrong et al., 2002) with two sinking classes: a) a soft (unprotected) POC that remineralizes at a fixed length scale (rate r = 0.016/d, sinking speed w = 3 m d^{-1}, l = 187.5 m) (b) a protected class strongly associated with mineral ballast types (biogenic silica and calcium carbonate), with deeper remineralization scales. Part of this class is converted to soft POC at each depth. $F_{\mathrm{POC}}(z)/\ F_{\mathrm{POC}}\ (z = z_0) = \exp(-(z - z_0)r/w)$ *Curve dominated by soft POC at mid-depths, and by ballast at a greater depth (sum of exponentials with different exponents).* *POC flux at 100 m is high in the tropics and high latitudes (Fig. S1), similar to observations. As a result of its more vigorous thermocline ventilation, ESM2M has higher total primary production and POC flux than ESM2G in most ocean areas.*	Switch to denitrification at O_2 < 5 mmol m^{-3} (with minimum nitrate condition NO_3> 0.1 mmol m^{-3}) Rate r_{denit} =0.002 d^{-1} (8 times less than oxic remineralization, l_{denit} = 1500 m) In the absence of both NO_3 and O_2, a respiration deficit is accumulated as negative O_2 (Dunne et al., 2013).	Diazotrophs fix dissolved N2 (with iron limitation).	All the remaining POC is remineralized on the bottom floor instantaneously (J. Dunne, personal communication, 2014).
HadGEM2-ES (CC)	POC flux in the form of slow-sinking detritus (10 m d^{-1}) with specific remineralization rate varying inversely with depth (Martin-style power law, but capped). $F_{\mathrm{POC}}(z)/\ F_{\mathrm{POC}}\ (z = z_0) = (z/z_0)^{-b}$ *Consistent with a power-law curve (below 100 m), with exponent b equal to 0.7 (Fig. 6).* *POC flux at 100 m follows the expected patterns (Fig. S1). However, low POC in the eastern tropical Pacific contributes to positive biases in oxygen in the OMZ regions.*	No denitrification	No nitrogen fixation	All detrital material reaching the sea floor is instantly remineralized. Newly remineralized material is spread evenly over lowest three layers. Sinking diatoms that hit the sea floor die instantly, becoming detritus.
PISCES (IPSL-CM5A)	Two types of POC, POCs (small) and POCb (big). Only POCb changes sinking speed with depth. $F_{\mathrm{POC}}(z)/\ F_{\mathrm{POC}}\ (z = z_0) = (z/z_0)^{-b}$ *The total POC remineralization curve is the sum of two power laws, as big and small POC have different exponents.* *Change in POC approximately consistent with a power-law curve, with exponent b varying from 0.75 at intermediate depths to 0.5 at depth (obtained from Fig. 6).*	Remineralization changes linearly from oxic to anoxic (denitrification) at oxygen levels between 6 mmol m^{-3} (all oxic) and 1 mmol m^{-3} (all denitrification). The rate of denitrification is the same as the rate of oxic remineralization.	Nitrogen fixation is parameterized in a crude way. – It is restricted to warm waters above 20° C. – It is restricted to area with insufficient nitrogen fixation. – It requires iron. – It is restricted to the sea surface. – To ensure N conservation in the ocean, annual total nitrogen fixation should balance denitrification.	In PISCES, sinking organic matter is permanently buried below the sea floor, thereby preventing the accumulation of detritus and slow remineralization at the bottom.
HAMOCC (MPI-ESM, NorESM1-ME)	POC in the form of detritus (remineralization rate r = 0.025/d, sinking speed of detritus w = 5 m d^{-1}, l = 200 m) $F_{\mathrm{POC}}(z)/\ F_{\mathrm{POC}}\ (z = z_0) = \exp(-(z - z_0)r/w)$ *POC flux at 100 m is too high in the eastern side of the tropical Pacific for both MPI-ESM and NorESM1-ME (Fig. S1). This contributes to the formation of a large OMZ. In MPI-ESM, POC flux is also high in the western tropics.*	At low oxygen levels (O_2 < 0.5 mmol m^{-3}), switch to denitrification and sulfur reduction. Denitrification rate 0.005 /d (5 times less than oxic remineralization, l_{denit} =1000 m)	In nitrate-limited oligotrophic regions, the model assumes nitrogen fixation by cyanobacteria, which is parameterized as the relaxation of the nitrate concentration at surface layer to the available phosphate concentration, through Redfield ratio. In a stationary ocean, denitrification and nitrogen fixation are balanced.	The sediment model used is based on Heinze et al. (1999). Within the sediment, remineralization of organic material is described as in the water column: aerobic remineralization occurs as long as oxygen is available in pore water, taking into account that part of the sediments becomes unavailable at each time step.
MRI-ESM1	POC in the form of detritus (remineralization rate r = 0.048 day^{-1}, sinking speed of detritus w = 2 m day^{-1}, l = 41.66 m) $F_{\mathrm{POC}}(z)/\ F_{\mathrm{POC}}(z = z_0) = \exp(-(z - z_0)r/w)$ *POC flux at 100 m is too high in the tropics and eastern Pacific (Fig. S1), possibly due to high subsurface recycling of organic matter associated with overestimated nitrate.*	No denitrification	No nitrogen fixation	

The Supplement related to this article is available online at doi:10.5194/bg-12-5429-2015-supplement.

Acknowledgements. A. Cabré and I. Marinov acknowledge support by NASA ROSES grant NNX13AC92G and by a University of Pennsylvania Research Foundation grant. R. B. was sponsored by NOAA Grant NOAA-NA10OAR4310092. We would like to thank J. Dunne, S. Henson, and D. Siegel for sharing their data results.

Edited by: V. Garçon

References

Armstrong, R. A., Lee, C., Hedges, J. I., Honjo, S., and Wakeham, S. G.: A new, mechanistic model for organic carbon fluxes in the ocean based on the quantitative association of POC with ballast minerals, Deep-Sea Res. Pt. II, 49, 219–236, 2002.

Ascani, F., Firing, E., Dutrieux, P., McCreary, J. P., and Ishida, A.: Deep Equatorial Ocean Circulation Induced by a Forced-Dissipated Yanai Beam, J. Phys. Oceanogr., 40, 1118–1142, doi:10.1175/2010jpo4356.1, 2010.

Assmann, K. M., Bentsen, M., Segschneider, J., and Heinze, C.: An isopycnic ocean carbon cycle model, Geosci. Model Dev., 3, 143–167, doi:10.5194/gmd-3-143-2010, 2010.

Aumont, O. and Bopp, L.: Globalizing results from ocean in situ iron fertilization studies, Global Biogeochem. Cy., 20, GB2017, doi:10.1029/2005gb002591, 2006.

Aumont, O., Orr, J. C., Monfray, P., Madec, G., and Maier-Reimer, E.: Nutrient trapping in the equatorial Pacific: The ocean circulation solution, Global Biogeochem. Cy., 13, 351–369, 1999.

Bentsen, M., Bethke, I., Debernard, J. B., Iversen, T., Kirkevåg, A., Seland, Ø., Drange, H., Roelandt, C., Seierstad, I. A., Hoose, C., and Kristjánsson, J. E.: The Norwegian Earth System Model, NorESM1-M – Part 1: Description and basic evaluation of the physical climate, Geosci. Model Dev., 6, 687–720, doi:10.5194/gmd-6-687-2013, 2013.

Bernardello, R., Marinov, I., Palter, J. B., Sarmiento, J. L., Galbraith, E. D., and Slater, R. D.: Response of the ocean natural carbon storage to projected twenty-first-century climate change, J. Climate, 27, 2033–2053, doi:10.1175/JCLI-D-13-00343.1, 2014.

Bianchi, D., Dunne, J. P., Sarmiento, J. L., and Galbraith, E. D.: Data-based estimates of suboxia, denitrification, and N_2O production in the ocean and their sensitivities to dissolved O-2, Global Biogeochem. Cy., 26, GB2009, doi:10.1029/2011gb004209, 2012.

Bograd, S. J., Castro, C. G., Di Lorenzo, E., Palacios, D. M., Bailey, H., Gilly, W., and Chavez, F. P.: Oxygen declines and the shoaling of the hypoxic boundary in the California Current, Geophys. Res. Lett., 35, L12607, doi:10.1029/2008gl034185, 2008.

Bopp, L., Le Quere, C., Heimann, M., Manning, A. C., and Monfray, P.: Climate-induced oceanic oxygen fluxes: Implications for the contemporary carbon budget, Global Biogeochem. Cy., 16, 6-1–6-13, doi:10.1029/2001gb001445, 2002.

Bopp, L., Resplandy, L., Orr, J. C., Doney, S. C., Dunne, J. P., Gehlen, M., Halloran, P., Heinze, C., Ilyina, T., Séférian, R., Tjiputra, J., and Vichi, M.: Multiple stressors of ocean ecosystems in the 21st century: projections with CMIP5 models, Biogeosciences, 10, 6225–6245, doi:10.5194/bg-10-6225-2013, 2013.

Brandt, P., Hormann, V., Bourles, B., Fischer, J., Schott, F. A., Stramma, L., and Dengler, M.: Oxygen tongues and zonal currents in the equatorial Atlantic, J. Geophys. Res.-Oceans, 113, C04012, doi:10.1029/2007jc004435, 2008.

Cabré, A., Marinov, I., and Leung, S.: Consistent global responses of marine ecosystems to future climate change across the IPCC AR5 Earth System Models, Clim. Dynam., 45, 5–6, 1253–1280, doi:10.1007/s00382-014-2374-3, 2015.

Chan, F., Barth, J. A., Lubchenco, J., Kirincich, A., Weeks, H., Peterson, W. T., and Menge, B. A.: Emergence of anoxia in the California current large marine ecosystem, Science, 319, 920–920, doi:10.1126/science.1149016, 2008.

Cocco, V., Joos, F., Steinacher, M., Frölicher, T. L., Bopp, L., Dunne, J., Gehlen, M., Heinze, C., Orr, J., Oschlies, A., Schneider, B., Segschneider, J., and Tjiputra, J.: Oxygen and indicators of stress for marine life in multi-model global warming projections, Biogeosciences, 10, 1849–1868, doi:10.5194/bg-10-1849-2013, 2013.

Collins, W. J., Bellouin, N., Doutriaux-Boucher, M., Gedney, N., Halloran, P., Hinton, T., Hughes, J., Jones, C. D., Joshi, M., Liddicoat, S., Martin, G., O'Connor, F., Rae, J., Senior, C., Sitch, S., Totterdell, I., Wiltshire, A., and Woodward, S.: Development and evaluation of an Earth-System model – HadGEM2, Geosci. Model Dev., 4, 1051–1075, doi:10.5194/gmd-4-1051-2011, 2011.

Czeschel, R., Stramma, L., and Johnson, G. C.: Oxygen decreases and variability in the eastern equatorial Pacific, J. Geophys. Res.-Oceans, 117, C11019, doi:10.1029/2012jc008043, 2012.

Danabasoglu, G., Bates, S. C., Briegleb, B. P., Jayne, S. R., Jochum, M., Large, W. G., Peacock, S., and Yeager, S. G.: The CCSM4 Ocean Component, J. Climate, 25, 1361–1389, doi:10.1175/jcli-d-11-00091.1, 2012.

Deutsch, C., Brix, H., Ito, T., Frenzel, H., and Thompson, L.: Climate-Forced Variability of Ocean Hypoxia, Science, 333, 336–339, doi:10.1126/science.1202422, 2011.

Deutsch, C., Berelson, W., Thunell, R., Weber, T., Tems, C., McManus, J., Crusius, J., Ito, T., Baumgartner, T., Ferreira, V., Mey, J., and van Geen, A.: OCEANOGRAPHY Centennial changes in North Pacific anoxia linked to tropical trade winds, Science, 345, 665–668, doi:10.1126/science.1252332, 2014.

Dietze, H. and Loeptien, U.: Revisiting "nutrient trapping" in global coupled biogeochemical ocean circulation models, Global Biogeochem. Cy., 27, 265–284, doi:10.1002/gbc.20029, 2013.

Downes, S. M., Bindoff, N. L., and Rintoul, S. R.: Changes in the Subduction of Southern Ocean Water Masses at the End of the Twenty-First Century in Eight IPCC Models, J. Climate, 23, 6526–6541, doi:10.1175/2010jcli3620.1, 2010.

Dufresne, J. L., Foujols, M. A., Denvil, S., Caubel, A., Marti, O., Aumont, O., Balkanski, Y., Bekki, S., Bellenger, H., Benshila, R., Bony, S., Bopp, L., Braconnot, P., Brockmann, P., Cadule, P., Cheruy, F., Codron, F., Cozic, A., Cugnet, D., de Noblet, N., Duvel, J. P., Ethe, C., Fairhead, L., Fichefet, T., Flavoni, S., Friedlingstein, P., Grandpeix, J. Y., Guez, L., Guilyardi, E., Hauglustaine, D., Hourdin, F., Idelkadi, A., Ghattas, J., Joussaume, S., Kageyama, M., Krinner, G., Labetoulle, S., Lahel-

lec, A., Lefebvre, M. P., Lefevre, F., Levy, C., Li, Z. X., Lloyd, J., Lott, F., Madec, G., Mancip, M., Marchand, M., Masson, S., Meurdesoif, Y., Mignot, J., Musat, I., Parouty, S., Polcher, J., Rio, C., Schulz, M., Swingedouw, D., Szopa, S., Talandier, C., Terray, P., Viovy, N., and Vuichard, N.: Climate change projections using the IPSL-CM5 Earth System Model: from CMIP3 to CMIP5, Clim. Dynam., 40, 2123–2165, doi:10.1007/s00382-012-1636-1, 2013.

Dunne, J. P., Armstrong, R. A., Gnanadesikan, A., and Sarmiento, J. L.: Empirical and mechanistic models for the particle export ratio, Global Biogeochem. Cy., 19, GB4026, doi:10.1029/2004gb002390, 2005.

Dunne, J. P., John, J. G., Adcroft, A. J., Griffies, S. M., Hallberg, R. W., Shevliakova, E., Stouffer, R. J., Cooke, W., Dunne, K. A., Harrison, M. J., Krasting, J. P., Malyshev, S. L., Milly, P. C. D., Phillipps, P. J., Sentman, L. T., Samuels, B. L., Spelman, M. J., Winton, M., Wittenberg, A. T., and Zadeh, N.: GFDL's ESM2 Global Coupled Climate-Carbon Earth System Models. Part I: Physical Formulation and Baseline Simulation Characteristics, J. Climate, 25, 6646–6665, doi:10.1175/jcli-d-11-00560.1, 2012.

Dunne, J. P., John, J. G., Shevliakova, E., Stouffer, R. J., Krasting, J. P., Malyshev, S. L., Milly, P. C. D., Sentman, L. T., Adcroft, A. J., Cooke, W., Dunne, K. A., Griffies, S. M., Hallberg, R. W., Harrison, M. J., Levy, H., Wittenberg, A. T., Phillips, P. J., and Zadeh, N.: GFDL's ESM2 Global Coupled Climate-Carbon Earth System Models. Part II: Carbon System Formulation and Baseline Simulation Characteristics, J. Climate, 26, 2247–2267, doi:10.1175/jcli-d-12-00150.1, 2013.

Duteil, O. and Oschlies A.: Sensitivity of simulated extent and future evolution of marine suboxia to mixing intensity, Geophys. Res. Lett., 38, L06607, doi::10.1029/2011GL046877, 2011.

Duteil, O., Schwarzkopf, F. U., Boning, C. W., and Oschlies, A.: Major role of the equatorial current system in setting oxygen levels in the eastern tropical Atlantic Ocean: A high-resolution model study, Geophys. Res. Lett., 41, 2033–2040, doi:10.1002/2013gl058888, 2014a.

Duteil, O., Böning, C. W., and Oschlies, A.: Variability in subtropical-tropical cells drives oxygen levels in the tropical Pacific Ocean, Geophys. Res. Lett., 41, 8926–8934, doi:10.1002/2014GL061774, 2014b.

Eden, C., and Dengler, M.: Stacked jets in the deep equatorial Atlantic Ocean, J. Geophys. Res.-Oceans, 113, C04003, doi:10.1029/2007jc004298, 2008.

Emerson, S., Watanabe, Y. W., Ono, T., and Mecking, S.: Temporal trends in apparent oxygen utilization in the upper pycnocline of the North Pacific: 1980–2000, J. Oceanogr., 60, 139–147, doi:10.1023/B:JOCE.0000038323.62130.a0, 2004.

Friedlingstein, P., Meinshausen, M., Arora, V. K., Jones, C. D., Anav, A., Liddicoat, S. K., and Knutti, R.: Uncertainties in CMIP5 Climate Projections due to Carbon Cycle Feedbacks, J. Climate, 27, 511–526, doi:10.1175/jcli-d-12-00579.1, 2014.

Fuenzalida, R., Schneider, W., Garces-Vargas, J., Bravo, L., and Lange, C.: Vertical and horizontal extension of the oxygen minimum zone in the eastern South Pacific Ocean, Deep-Sea Res. Pt. II, 56, 1027–1038, doi:10.1016/j.dsr2.2008.11.001, 2009.

Garcia, H. E. and Gordon, L. I.: oxygen solubility in seawater – better fitting equations, Limnol. Oceanogr., 37, 1307–1312, 1992.

Gent, P. R., Danabasoglu, G., Donner, L. J., Holland, M. M., Hunke, E. C., Jayne, S. R., Lawrence, D. M., Neale, R. B., Rasch, P. J., Vertenstein, M., Worley, P. H., Yang, Z. L., and Zhang, M. H.: The Community Climate System Model Version 4, J. Climate, 24, 4973–4991, doi:10.1175/2011jcli4083.1, 2011.

Getzlaff, J., and Dietze, H.: Effects of increased isopycnal diffusivity mimicking the unresolved equatorial intermediate current system in an earth system climate model, Geophys. Res. Lett., 40, 2166–2170, doi:10.1002/grl.50419, 2013.

Giorgetta, M. A., Jungclaus, J., Reick, C. H., Legutke, S., Bader, J., Bottinger, M., Brovkin, V., Crueger, T., Esch, M., Fieg, K., Glushak, K., Gayler, V., Haak, H., Hollweg, H. D., Ilyina, T., Kinne, S., Kornblueh, L., Matei, D., Mauritsen, T., Mikolajewicz, U., Mueller, W., Notz, D., Pithan, F., Raddatz, T., Rast, S., Redler, R., Roeckner, E., Schmidt, H., Schnur, R., Segschneider, J., Six, K. D., Stockhause, M., Timmreck, C., Wegner, J., Widmann, H., Wieners, K. H., Claussen, M., Marotzke, J., and Stevens, B.: Climate and carbon cycle changes from 1850 to 2100 in MPI-ESM simulations for the Coupled Model Intercomparison Project phase 5, J. Adv. Model. Earth Sys., 5, 572–597, doi:10.1002/jame.20038, 2013.

Gnanadesikan, A., Russell, J. L., and Zeng, F.: How does ocean ventilation change under global warming?, Ocean Science, 3, 43–53, 2007.

Gnanadesikan, A., Dunne, J. P., and John, J.: Understanding why the volume of suboxic waters does not increase over centuries of global warming in an Earth System Model, Biogeosciences, 9, 1159–1172, doi:10.5194/bg-9-1159-2012, 2012.

Gnanadesikan, A., Bianchi, D., and Pradal, M. A.: Critical role for mesoscale eddy diffusion in supplying oxygen to hypoxic ocean waters, Geophys. Res. Lett., 40, 5194–5198, doi:10.1002/grl.50998, 2013.

Gray, J. S., Wu, R. S. S., and Or, Y. Y.: Effects of hypoxia and organic enrichment on the coastal marine environment, Mar. Ecol.-Prog.Ser., 238, 249–279, doi:10.3354/meps238249, 2002.

Hansell, D. A.: Recalcitrant dissolved organic carbon fractions, Annu. Rev. Mar. Sci., 5, 421–445, doi:10.1146/annurev-marine-120710-100757, 2013.

Helm, K. P., Bindoff, N. L., and Church, J. A.: Observed decreases in oxygen content of the global ocean, Geophys. Res. Lett., 38, L23602, doi:10.1029/2011gl049513, 2011.

Henson, S. A., Sanders, R., and Madsen, E.: Global patterns in efficiency of particulate organic carbon export and transfer to the deep ocean, Global Biogeochem. Cy., 26, GB1028, doi:10.1029/2011gb004099, 2012.

The HadGEM2 Development Team: Martin, G. M., Bellouin, N., Collins, W. J., Culverwell, I. D., Halloran, P. R., Hardiman, S. C., Hinton, T. J., Jones, C. D., McDonald, R. E., McLaren, A. J., O'Connor, F. M., Roberts, M. J., Rodriguez, J. M., Woodward, S., Best, M. J., Brooks, M. E., Brown, A. R., Butchart, N., Dearden, C., Derbyshire, S. H., Dharssi, I., Doutriaux-Boucher, M., Edwards, J. M., Falloon, P. D., Gedney, N., Gray, L. J., Hewitt, H. T., Hobson, M., Huddleston, M. R., Hughes, J., Ineson, S., Ingram, W. J., James, P. M., Johns, T. C., Johnson, C. E., Jones, A., Jones, C. P., Joshi, M. M., Keen, A. B., Liddicoat, S., Lock, A. P., Maidens, A. V., Manners, J. C., Milton, S. F., Rae, J. G. L., Ridley, J. K., Sellar, A., Senior, C. A., Totterdell, I. J., Verhoef, A., Vidale, P. L., and Wiltshire, A.: The HadGEM2 family of Met Office Unified Model climate configurations, Geosci. Model Dev., 4, 723–757, doi:10.5194/gmd-4-723-2011, 2011.

Ilyina, T., Six, K. D., Segschneider, J., Maier-Reimer, E., Li, H. M., and Nunez-Riboni, I.: Global ocean biogeochemistry model HAMOCC: Model architecture and performance as component of the MPI-Earth system model in different CMIP5 experimental realizations, J. Adv. Model. Earth Sys., 5, 287–315, doi:10.1029/2012ms000178, 2013.

Ito, T. and Deutsch, C.: Variability of the oxygen minimum zone in the tropical North Pacific during the late twentieth century, Global Biogeochem. Cy., 27, 1119–1128, doi:10.1002/2013gb004567, 2013.

Ito, T., Follows, M. J., and Boyle, E. A.: Is AOU a good measure of respiration in the oceans?, Geophys. Res. Lett., 31, L17305, doi:10.1029/2004gl020900, 2004.

Iversen, T., Bentsen, M., Bethke, I., Debernard, J. B., Kirkevåg, A., Seland, Ø., Drange, H., Kristjansson, J. E., Medhaug, I., Sand, M., and Seierstad, I. A.: The Norwegian Earth System Model, NorESM1-M – Part 2: Climate response and scenario projections, Geosci. Model Dev., 6, 389–415, doi:10.5194/gmd-6-389-2013, 2013.

Johnson, G. C., Sloyan, B. M., Kessler, W. S., and McTaggart, K. E.: Direct measurements of upper ocean currents and water properties across the tropical Pacific during the 1990s, Prog. Oceanogr., 52, 31–61, doi:10.1016/s0079-6611(02)00021-6, 2002.

Jones, C. D., Hughes, J. K., Bellouin, N., Hardiman, S. C., Jones, G. S., Knight, J., Liddicoat, S., O'Connor, F. M., Andres, R. J., Bell, C., Boo, K.-O., Bozzo, A., Butchart, N., Cadule, P., Corbin, K. D., Doutriaux-Boucher, M., Friedlingstein, P., Gornall, J., Gray, L., Halloran, P. R., Hurtt, G., Ingram, W. J., Lamarque, J.-F., Law, R. M., Meinshausen, M., Osprey, S., Palin, E. J., Parsons Chini, L., Raddatz, T., Sanderson, M. G., Sellar, A. A., Schurer, A., Valdes, P., Wood, N., Woodward, S., Yoshioka, M., and Zerroukat, M.: The HadGEM2-ES implementation of CMIP5 centennial simulations, Geosci. Model Dev., 4, 543–570, doi:10.5194/gmd-4-543-2011, 2011.

Jungclaus, J. H., Fischer, N., Haak, H., Lohmann, K., Marotzke, J., Matei, D., Mikolajewicz, U., Notz, D., and von Storch, J. S.: Characteristics of the ocean simulations in the Max Planck Institute Ocean Model (MPIOM) the ocean component of the MPI-Earth system model, J. Adv. Model. Earth Sys., 5, 422–446, doi:10.1002/jame.20023, 2013.

Kaplan, A., Kushnir, Y., and Cane, M. A.: Reduced space optimal interpolation of historical marine sea level pressure: 1854–1992, J. Climate, 13, 2987–3002, doi:10.1175/1520-0442(2000)013_2987:rsoioh_2.0.co;2, 2000.

Karstensen, J., Stramma, L., and Visbeck, M.: Oxygen minimum zones in the eastern tropical Atlantic and Pacific oceans, Prog. Oceanogr., 77, 331–350, doi:10.1016/j.pocean.2007.05.009, 2008.

Keeling, R. F. and Garcia, H. E.: The change in oceanic O-2 inventory associated with recent global warming, P. Natl. Acad. Sci. USA, 99, 7848–7853, doi:10.1073/pnas.122154899, 2002.

Keeling, R. F., Kortzinger, A., and Gruber, N.: Ocean Deoxygenation in a Warming World, Annual Review of Marine Science, 2, 199–229, doi:10.1146/annurev.marine.010908.163855, 2010.

Kriest, I. and Oschlies, A.: Swept under the carpet: organic matter burial decreases global ocean biogeochemical model sensitivity to remineralization length scale, Biogeosciences, 10, 8401–8422, doi:10.5194/bg-10-8401-2013, 2013.

Kriest, I., Khatiwala, S., and Oschlies, A.: Towards an assessment of simple global marine biogeochemical models of different complexity, Prog. Oceanogr., 86, 337–360, doi:10.1016/j.pocean.2010.05.002, 2010.

Kriest, I., Oschlies, A., and Khatiwala, S.: Sensitivity analysis of simple global marine biogeochemical models, Global Biogeochem. Cy., 26, GB2029, doi:10.1029/2011gb004072, 2012.

Landolfi, A., Dietze, H., Koeve, W., and Oschlies, A.: Overlooked runaway feedback in the marine nitrogen cycle: the vicious cycle, Biogeosciences, 10, 1351–1363, doi:10.5194/bg-10-1351-2013, 2013.

Li, G., and Xie, S. P.: Tropical Biases in CMIP5 Multimodel Ensemble: The Excessive Equatorial Pacific Cold Tongue and Double ITCZ Problems, J. Climate, 27, 1765–1780, doi:10.1175/jcli-d-13-00337.1, 2014.

Lin, J.: The Double-ITCZ Problem in IPCC AR4 Coupled GCMs: Ocean-Atmosphere Feedback Analysis, J. Climate, 20, 4497–4525, doi:10.1175/JCLI4272.1, 2007.

Lindsay, K., Bonan, G. B., Doney, S. C., Hoffman, F. M., Lawrence, D. M., Long, M. C., Mahowald, N. M., Moore, J. K., Randerson, J. T., and Thornton, P. E.: Preindustrial-Control and Twentieth-Century Carbon Cycle Experiments with the Earth System Model CESM1(BGC), J. Climate, 27, 8981–9005, doi:10.1175/JCLI-D-12-00565.1, 2014.

Llanillo, P. J., Karstensen, J., Pelegrí, J. L., and Stramma, L.: Physical and biogeochemical forcing of oxygen and nitrate changes during El Niño/El Viejo and La Niña/La Vieja upper-ocean phases in the tropical eastern South Pacific along 86° W, Biogeosciences, 10, 6339–6355, doi:10.5194/bg-10-6339-2013, 2013.

Lübbecke, J. F., Böning, C. W., and Biastoch, A.: Variability in the subtropical-tropical cells and its effect on near-surface temperature of the equatorial Pacific: a model study, Ocean Sci., 4, 73–88, doi:10.5194/os-4-73-2008, 2008.

Marsay, C. M., Sanders, R. J., Henson, S. A., Pabortsava, K., Achterberg, E. P., and Lampitt, R. S.: Attenuation of sinking particulate organic carbon flux through the mesopelagic ocean, P. Natl. Acad. Sci. USA, 112, 4, 1089–1094, doi:10.1073/pnas.1415311112, 2014.

Martin, J. H., Knauer, G. A., Karl, D. M., and Broenkow, W. W.: VERTEX – Carbon cycling in the northeast pacific, Deep-Sea Res. Pt. I, 34, 267–285, doi:10.1016/0198-0149(87)90086-0, 1987.

Matear, R. J. and Hirst, A. C.: Long-term changes in dissolved oxygen concentrations in the ocean caused by protracted global warming, Global Biogeochem. Cy., 17, 1125, doi:10.1029/2002gb001997, 2003.

McClatchie, S., Goericke, R., Cosgrove, R., Auad, G., and Vetter, R.: Oxygen in the Southern California Bight: Multidecadal trends and implications for demersal fisheries, Geophys. Res. Lett., 37, L19602, doi:10.1029/2010gl044497, 2010.

Meijers, A. J. S.: The Southern Ocean in the Coupled Model Intercomparison Project phase 5, Philos. T. R. Soc. A, 372, 2019, doi:10.1098/rsta.2013.0296, 2014.

Meinshausen, M., Smith, S. J., Calvin, K., Daniel, J. S., Kainuma, M. L. T., Lamarque, J. F., Matsumoto, K., Montzka, S. A., Raper, S. C. B., Riahi, K., Thomson, A., Velders, G. J. M., and van Vuuren, D. P. P.: The RCP greenhouse gas concentrations and their extensions from 1765 to 2300, Climatic Change, 109, 213–241, doi:10.1007/s10584-011-0156-z, 2011.

Montes, I., Dewitte, B., Gutknecht, E., Paulmier, A., Dadou, I., Oschlies, A., and Garcon, V.: High-resolution modeling of the Eastern Tropical Pacific oxygen minimum zone: Sensitivity to the tropical oceanic circulation, J. Geophys. Res.-Oceans, 119, 5515–5532, doi:10.1002/2014jc009858, 2014.

Moore, J. K. and Doney, S. C.: Iron availability limits the ocean nitrogen inventory stabilizing feedbacks between marine denitrification and nitrogen fixation, Global Biogeochem. Cy., 21, GB2001, doi:10.1029/2006gb002762, 2007.

Moore, J. K., Doney, S. C., and Lindsay, K.: Upper ocean ecosystem dynamics and iron cycling in a global three-dimensional model, Global Biogeochem. Cy., 18, GB4028, doi:10.1029/2004gb002220, 2004.

Moore, J. K., Doney, S. C., Lindsay, K., Mahowald, N., and Michaels, A. F.: Nitrogen fixation amplifies the ocean biogeochemical response to decadal timescale variations in mineral dust deposition, Tellus B, 58, 560–572, doi:10.1111/j.1600-0889.2006.00209.x, 2006.

Moore, J. K., Lindsay, K., Doney, S. C., Long, M. C., and Misumi, K.: Marine Ecosystem Dynamics and Biogeochemical Cycling in the Community Earth System Model CESM1(BGC) : Comparison of the 1990s with the 2090s under the RCP4.5 and RCP8.5 Scenarios, J. Climate, 26, 9291–9312, doi:10.1175/jcli-d-12-00566.1, 2013.

Najjar, R. G., Sarmiento, J. L., and Toggweiler, J. R.: Downward transport and fate of organic matter in the ocean: simulations with a general circulation model, Global Biogeochem. Cy., 6, 45–76, doi:10.1029/91GB02718, 1992.

Najjar, R. G., Jin, X., Louanchi, F., Aumont, O., Caldeira, K., Doney, S. C., Dutay, J. C., Follows, M., Gruber, N., Joos, F., Lindsay, K., Maier-Reimer, E., Matear, R. J., Matsumoto, K., Monfray, P., Mouchet, A., Orr, J. C., Plattner, G. K., Sarmiento, J. L., Schlitzer, R., Slater, R. D., Weirig, M. F., Yamanaka, Y., and Yool, A.: Impact of circulation on export production, dissolved organic matter, and dissolved oxygen in the ocean: Results from Phase II of the Ocean Carbon-cycle Model Intercomparison Project (OCMIP-2), Global Biogeochem. Cy., 21, GB3007, doi:10.1029/2006gb002857, 2007.

Ono, T., Midorikawa, T., Watanabe, Y. W., Tadokoro, K., and Saino, T.: Temporal increases of phosphate and apparent oxygen utilization in the subsurface waters of western subarctic Pacific from 1968 to 1998, Geophys. Res. Lett., 28, 3285–3288, doi:10.1029/2001gl012948, 2001.

Palmer, J. R. and Totterdell, I. J.: Production and export in a global ocean ecosystem model, Deep-Sea Res. Pt. I, 48, 1169–1198, doi:10.1016/s0967-0637(00)00080-7, 2001.

Paulmier, A. and Ruiz-Pino, D.: Oxygen minimum zones (OMZs) in the modern ocean, Prog. Oceanogr., 80, 113–128, doi:10.1016/j.pocean.2008.08.001, 2009.

Pierce, S. D., Barth, J. A., Shearman, R. K., and Erofeev, A. Y.: Declining Oxygen in the Northeast Pacific, J. Phys. Oceanogr., 42, 495–501, doi:10.1175/jpo-d-11-0170.1, 2012.

Riahi, K., Rao, S., Krey, V., Cho, C., Chirkov, V., Fischer, G., Kindermann, G., Nakicenovic, N., and Rafaj, P.: RCP 8.5-A scenario of comparatively high greenhouse gas emissions, Climatic Change, 109, 33–57, doi:10.1007/s10584-011-0149-y, 2011.

Ridder, N. N. and England, M. H.: Sensitivity of ocean oxygenation to variations in tropical zonal wind stress magnitude, Global Biogeochem. Cy., 28, 909–926, doi:10.1002/2013gb004708, 2014.

Sallee, J. B., Shuckburgh, E., Bruneau, N., Meijers, A. J. S., Bracegirdle, T. J., and Wang, Z.: Assessment of Southern Ocean mixed-layer depths in CMIP5 models: Historical bias and forcing response, J. Geophys. Res.-Oceans, 118, 1845–1862, doi:10.1002/jgrc.20157, 2013a.

Sallee, J. B., Shuckburgh, E., Bruneau, N., Meijers, A. J. S., Bracegirdle, T. J., Wang, Z., and Roy, T.: Assessment of Southern Ocean water mass circulation and characteristics in CMIP5 models: Historical bias and forcing response, J. Geophys. Res.-Oceans, 118, 1830–1844, doi:10.1002/jgrc.20135, 2013b.

Sandeep, S., Stordal, F., Sardeshmukh, P. D., and Compo, G. P.: Pacific Walker Circulation variability in coupled and uncoupled climate models, Climate Dynamics, 43, 1, 103–117, doi:10.1007/s00382-014-2135-3, 2014

Seferian, R., Bopp, L., Gehlen, M., Orr, J. C., Ethe, C., Cadule, P., Aumont, O., Melia, D. S. Y., Voldoire, A., and Madec, G.: Skill assessment of three earth system models with common marine biogeochemistry, Clim. Dynam., 40, 2549–2573, doi:10.1007/s00382-012-1362-8, 2013.

Seibel, B. A.: Critical oxygen levels and metabloic suppression in oceanic oxygen minimum zones, J. Exp. Biol., 214, 326–336, doi:10.1242/jeb.049171, 2011.

Sen Gupta, A., Santoso, A., Taschetto, A. S., Ummenhofer, C. C., Trevena, J., and England, M. H.: Projected Changes to the Southern Hemisphere Ocean and Sea Ice in the IPCC AR4 Climate Models, J. Climate, 22, 3047–3078, doi:10.1175/2008jcli2827.1, 2009.

Siegel, D. A., Buesseler, K. O., Doney, S. C., Sailley, S. F., Behrenfeld, M. J., and Boyd, P. W.: Global assessment of ocean carbon export by combining satellite observations and food-web models, Global Biogeochem. Cy., 28, 181–196, doi:10.1002/2013gb004743, 2014.

Stramma, L., Johnson, G. C., Sprintall, J., and Mohrholz, V.: Expanding oxygen-minimum zones in the tropical oceans, Science, 320, 655–658, doi:10.1126/science.1153847, 2008.

Stramma, L., Johnson, G. C., Firing, E., and Schmidtko, S.: Eastern Pacific oxygen minimum zones: Supply paths and multidecadal changes, J. Geophys. Res.-Oceans, 115, C09011, doi:10.1029/2009jc005976, 2010a.

Stramma, L., Schmidtko, S., Levin, L. A., and Johnson, G. C.: Ocean oxygen minima expansions and their biological impacts, Deep-Sea Res. Pt. I, 57, 587–595, doi:10.1016/j.dsr.2010.01.005, 2010b.

Stramma, L., Oschlies, A., and Schmidtko, S.: Mismatch between observed and modeled trends in dissolved upper-ocean oxygen over the last 50 yr, Biogeosciences, 9, 4045–4057, doi:10.5194/bg-9-4045-2012, 2012.

Taylor, K. E., Stouffer, R. J., and Meehl, G. A.: an overview of cmip5 and the experiment design, B. Am. Meteorol. Soc., 93, 485–498, doi:10.1175/bams-d-11-00094.1, 2012.

Tjiputra, J. F., Roelandt, C., Bentsen, M., Lawrence, D. M., Lorentzen, T., Schwinger, J., Seland, Ø., and Heinze, C.: Evaluation of the carbon cycle components in the Norwegian Earth System Model (NorESM), Geosci. Model Dev., 6, 301–325, doi:10.5194/gmd-6-301-2013, 2013.

Tsuchiya, M.: THE ORIGIN OF THE PACIFIC EQUATORIAL 13-DEGREES-C WATER, J. Phys. Oceanogr., 11, 794–812, doi:10.1175/1520-0485(1981)011< 0794:tootpe> 2.0.co;2, 1981.

Vecchi, G. A., Soden, B. J., Wittenberg, A. T., Held, I. M., Leetmaa, A., and Harrison, M. J.: Weakening of tropical Pacific atmospheric circulation due to anthropogenic forcing, Nature, 441, 73–76, doi:10.1038/nature04744, 2006.

Weijer, W., Sloyan, B. M., Maltrud, M. E., Jeffery, N., Hecht, M. W., Hartin, C. A., van Sebille, E., Wainer, I., and Landrum, L.: The Southern Ocean and Its Climate in CCSM4, J. Climate, 25, 2652–2675, doi:10.1175/jcli-d-11-00302.1, 2012.

Whitney, F. A., Freeland, H. J., and Robert, M.: Persistently declining oxygen levels in the interior waters of the eastern subarctic Pacific, Prog. Oceanogr., 75, 179–199, doi:10.1016/j.pocean.2007.08.007, 2007.

Williams, J. H. T., Totterdell, I. J., Halloran, P. R., and Valdes, P. J.: Numerical simulations of oceanic oxygen cycling in the FAMOUS Earth-System model: FAMOUS-ES, version 1.0, Geosci. Model Dev., 7, 1419–1431, doi:10.5194/gmd-7-1419-2014, 2014.

Yukimoto, S., Yoshimura, H., Hosaka, M., Sakami, T., Tsujino, H., Hirabara, M., Tanaka, T.Y., Deushi, M., Obata, A., Nakano, H., Adachi, Y., Shindo, E., Yabu, S., Ose, T., and Kitoh, A.: Meteorological Research Institute-Earth System Model Version 1 (MRI-ESM1) Model Description, Technical Reports of the Meteorological Research Institute No. 64, 2011.